REFERENCES

[1] Baig N, Kammakakam I, Falath W and Kammakakam I 2021 Nanomaterials: A review of synthesis methods, properties, recent progress, and challenges *Mater. Adv.* **2** 1821–71

[2] Chow J C L 2022 Special Issue: Application of Nanomaterials in Biomedical Imaging and Cancer Therapy *Nanomaterials* **12** 1–40

[3] Shah J, Pandya A, Goyal P, Misra S K and Singh S 2020 BSA-Decorated Magnesium Nanoparticles for Scavenging Hydrogen Peroxide from Human Hepatic Cells *ACS Appl. Nano Mater.* **3** 3355–70

[4] Elansary M, Belaiche M, Mouhib Y, Lemine O M, Bentarhlia N and Bsoul I 2023 Novel biocompatible nanomaterial for biomedical application: Structural, morphological, magnetic, and in vivo toxicity investigations *Ceram. Int.* **49** 4551–70

[5] Wang C X and Yang G W 2005 Thermodynamics of metastable phase nucleation at the nanoscale *Mater. Sci. Eng. R Reports* **49** 157–202

[6] Verma V K, Sabbarwal S, Srivastava P and Kumar M 2023 In-depth insight of thermodynamic and kinetic barrier for computation of nucleation rate and interfacial energy of ultra-small Gd2O3 nanoclusters utilizing non-isothermal thermogravimetric models *Phys. Scr.* **98**

[7] Jha R, Diercks D R, Chakraborti N, Stebner A P and Ciobanu C V. 2019 Interfacial energy of copper clusters in Fe-Si-B-Nb-Cu alloys *Scr. Mater.* **162** 331–4

[8] Fernandez-Martinez A, Hu Y, Lee B, Jun Y S and Waychunas G A 2013 In situ determination of interfacial energies between heterogeneously nucleated CaCO3 and

quartz substrates: Thermodynamics of CO 2 mineral trapping *Environ. Sci. Technol.* **47** 102–9

[9] Srivastava P, Sabbarwal S, Verma V K and Kumar M 2023 A novel approach for determination of nucleation rates and interfacial energy of metallic magnesium nanoclusters at high temperature using non-isothermal TGA models *Chem. Eng. Sci.* **265** 118223

[10] Thakkar K N, Mhatre S S and Parikh R Y 2010 Biological synthesis of metallic nanoparticles *Nanomedicine Nanotechnology, Biol. Med.* **6** 257–62

[11] Vijayaram S, Razafindralambo H, Sun Y Z, Vasantharaj S, Ghafarifarsani H, Hoseinifar S H and Raeeszadeh M 2023 Applications of Green Synthesized Metal Nanoparticles — a Review *Biol. Trace Elem. Res.*

[12] Ali S, Sudha K G, Thirumalaivasan N, Ahamed M, Pandiaraj S, Rajeswari V D, Vinayagam Y, Thiruvengadam M and Govindasamy R 2023 Green Synthesis of Magnesium Oxide Nanoparticles by Using Abrus precatorius Bark Extract and Their Photocatalytic, Antioxidant, Antibacterial, and Cytotoxicity Activities *Bioengineering* **10**

[13] Iravani S, Korbekandi H, Mirmohammadi S V and Zolfaghari B 2014 Synthesis of silver nanoparticles: chemical, physicIravani, S., Korbekandi, H., Mirmohammadi, S. V, & Zolfaghari, B. (2014). Synthesis of silver nanoparticles: chemical, physical and biological methods. Research in Pharmaceutical Sciences, 9(6), 385–406. *Res. Pharm. Sci.* **9** 385–406

[14] Huang X, Li Z, Yu Z, Deng X, Xin Y and Jesionowski T 2019 Recent Advances in the Synthesis, Properties, and Biological Applications of Platinum Nanoclusters *J. Nanomater.* **2019**

[15] Moosavy M H, de la Guardia M, Mokhtarzadeh A, Khatibi S A, Hosseinzadeh N and Hajipour N 2023 Green synthesis, characterization, and biological evaluation of gold and silver nanoparticles using Mentha spicata essential oil *Sci. Rep.* **13** 1–15

[16] Yuan X, Luo Z, Zhang Q, Zhang X, Zheng Y, Lee J Y and Xie J 2011 Synthesis of highly fluorescent metal (Ag, Au, Pt, and Cu) nanoclusters by electrostatically induced reversible phase transfer *ACS Nano* **5** 8800–8

[17] Javed R, Zia M, Naz S, Aisida S O, ul Ain N and Ao Q 2020 Role of capping agents in the application of nanoparticles in biomedicine and environmental remediation: recent trends and future prospects *J. Nanobiotechnology* **18** 1–15

[18] Wu Z and Jin R 2010 On the ligand's role in the fluorescence of gold nanoclusters *Nano Lett.* **10** 2568–73

[19] Kathmann S M, Schenter G K, Garrett B C, Chen B and Siepmann J I 2009 Thermodynamics and kinetics of nanoclusters controlling gas-to-particle nucleation *J. Phys. Chem. C* **113** 10354–70

[20] Polte J 2015 Fundamental growth principles of colloidal metal nanoparticles - a new perspective *CrystEngComm* **17** 6809–30

[21] Klein D H, Smith M D and Driy J A 1967 Homogeneous nucleation of magnesium hydroxide *Talanta* **14** 937–40

[22] Bian J, Guo D, Li Y, Cai W, Hua Y and Cao X 2022 Homogeneous nucleation and condensation mechanism of methane gas: A molecular simulation perspective *Energy* **249** 123610

[23] Aguiar C das D, Coelho Y L, de Paula H M C, Santa Rosa L N, Virtuoso L S, Mendes T A de O, Pires A C dos S and da Silva L H M 2021 Thermodynamic and

kinetic insights into the interactions between functionalized CdTe quantum dots and human serum albumin: A surface plasmon resonance approach *Int. J. Biol. Macromol.* **184** 990–9

[24] Nafsin N, Aguiar J A, Aoki T, Thron A M, van Benthem K and Castro R H R 2017 Thermodynamics versus kinetics of grain growth control in nanocrystalline zirconia *Acta Mater.* **136** 224–34

[25] Gambinossi F, Mylon S E and Ferri J K 2015 Aggregation kinetics and colloidal stability of functionalized nanoparticles *Adv. Colloid Interface Sci.* **222** 332–49

[26] Pranjali P, Tripathi D K, Chaturvedi A, Singh R K, Poluri K M, Kumar D and Guleria A 2023 Role of surface hydrophilicity on MR relaxivity of PEG coated-gadolinium oxide nanoparticles *Phys. Scr.* **98**

[27] Khramtsov P, Barkina I, Kropaneva M, Bochkova M, Timganova V, Nechaev A, Byzov I, Zamorina S, Yermakov A and Rayev M 2019 Magnetic nanoclusters coated with albumin, casein, and gelatin: Size tuning, relaxivity, stability, protein corona, and application in nuclear magnetic resonance immunoassay *Nanomaterials* **9**

[28] Li Q, Fernandez-Martinez A, Lee B, Waychunas G A and Jun Y S 2014 Interfacial energies for heterogeneous nucleation of calcium carbonate on mica and quartz *Environ. Sci. Technol.* **48** 5745–53

[29] Hu Q, Nielsen M H, Freeman C L, Hamm L M, Tao J, Lee J R I, Han T Y J, Becker U, Harding J H, Dove P M and De Yoreo J J 2012 The thermodynamics of calcite nucleation at organic interfaces: Classical vs. non-classical pathways *Faraday Discuss.* **159** 509–23

[30] Elmizadeh H, Khanmohammadi M, Ghasemi K, Hassanzadeh G, Nassiri-Asl M and

Garmarudi A B 2013 Preparation and optimization of chitosan nanoparticles and magnetic chitosan nanoparticles as delivery systems using Box-Behnken statistical design *J. Pharm. Biomed. Anal.* **80** 141–6

[31] Wang L, Xing H, Zhang S, Ren Q, Pan L, Zhang K, Bu W, Zheng X, Zhou L, Peng W, Hua Y and Shi J 2013 A Gd-doped Mg-Al-LDH/Au nanocomposite for CT/MR bimodal imagings and simultaneous drug delivery *Biomaterials* **34** 3390–401

[32] Wang Q, Lv L, Ling Z, Wang Y, Liu Y, Li L, Liu G, Shen L, Yan J and Wang Y 2015 Long-circulating iodinated albumin-gadolinium nanoparticles as enhanced magnetic resonance and computed tomography imaging probes for osteosarcoma visualization *Anal. Chem.* **87** 4299–304

[33] Li Y, Feng L, Yan W, Hussain I, Su L and Tan B 2019 PVP-templated highly luminescent copper nanoclusters for sensing trinitrophenol and living cell imaging *Nanoscale* **11** 1286–94

[34] Ghisaidoobe A B T and Chung S J 2014 Intrinsic tryptophan fluorescence in the detection and analysis of proteins: A focus on förster resonance energy transfer techniques *Int. J. Mol. Sci.* **15** 22518–38

[35] Elansary M, Belaiche M, Mouhib Y, Lemine O M, Bentarhlia N and Bsoul I 2023 Novel biocompatible nanomaterial for biomedical application: Structural, morphological, magnetic, and in vivo toxicity investigations *Ceram. Int.* **49** 4551–70

[36] Fatima A, Ahmad M W, Al Saidi A K A, Choudhury A, Chang Y and Lee G H 2021 Recent advances in gadolinium based contrast agents for bioimaging applications *Nanomaterials* **11** 1–23

[37] Lillo C R, Calienni M N, Rivas Aiello B, Prieto M J, Rodriguez Sartori D, Tuninetti J, Toledo P, Alonso S del V, Moya S, Gonzalez M C, Montanari J and Soler-Illia G J A A 2020 BSA-capped gold nanoclusters as potential theragnostic for skin diseases: Photoactivation, skin penetration, in vitro, and in vivo toxicity *Mater. Sci. Eng. C* **112** 110891

[38] Zhao J, Zhang Q, Liu W, Shan G and Wang X 2021 Biocompatible BSA-Ag2S Nanoparticles for Photothermal Therapy of Cancer *Colloids Surfaces B Biointerfaces* **211** 112295

[39] Kuo S H, Chien C S, Wang C C and Shih C J 2019 Antibacterial activity of bsa-capped gold nanoclusters against methicillin-resistant staphylococcus aureus (mrsa) and vancomycin-intermediate Staphylococcus aureus (VISA) *J. Nanomater.* **2019**

[40] Arora N, Thangavelu K and Karanikolos G N 2020 Bimetallic Nanoparticles for Antimicrobial Applications *Front. Chem.* **8** 1–22

[41] Bankura K, Maity D, Mollick M M R, Mondal D, Bhowmick B, Roy I, Midya T, Sarkar J, Rana D, Acharya K and Chattopadhyay D 2014 Antibacterial activity of Ag-Au alloy NPs and chemical sensor property of Au NPs synthesized by dextran *Carbohydr. Polym.* **107** 151–7

[42] Tanaka S I, Wadati H, Sato K, Yasuda H and Niioka H 2020 Red-Fluorescent Pt Nanoclusters for Detecting and Imaging HER2 in Breast Cancer Cells *ACS Omega* **5** 23718–23

[43] Sahoo A K, Banerjee S, Ghosh S S and Chattopadhyay A 2014 Simultaneous RGB emitting Au nanoclusters in chitosan nanoparticles for anticancer gene theranostics *ACS Appl. Mater. Interfaces* **6** 712–24

[44] Chawda N, Mishra S, Basu M, Chander H, Podder R, Mahapatra S K and Banerjee I 2019 Synthesis of gadolinium oxide nanocuboids for in vitro bioimaging applications *Mater. Res. Express* **6**

[45] Anishur Rahman A T M, Vasilev K and Majewski P 2011 Ultra small Gd2O3 nanoparticles: Absorption and emission properties *J. Colloid Interface Sci.* **354** 592–6

[46] Liao W Y, Li H J, Chang M Y, Tang A C L, Hoffman A S and Hsieh P C H 2013 Comprehensive characterizations of nanoparticle biodistribution following systemic injection in mice *Nanoscale* **5** 11079–86

[47] Tsang V T C, Li X and Wong T T W 2020 A review of endogenous and exogenous contrast agents used in photoacoustic tomography with different sensing configurations *Sensors (Switzerland)* **20** 1–20

[48] Miller J P, Habimana-Griffin L, Edwards T S and Achilefu S 2017 Multimodal fluorescence molecular imaging for in vivo characterization of skin cancer using endogenous and exogenous fluorophores *J. Biomed. Opt.* **22** 066007

[49] Sato K, Gorka A P, Nagaya T, Michie M S, Nani R R, Nakamura Y, Coble V L, Vasalatiy O V., Swenson R E, Choyke P L, Schnermann M J and Kobayashi H 2016 Role of Fluorophore Charge on the in Vivo Optical Imaging Properties of Near-Infrared Cyanine Dye/Monoclonal Antibody Conjugates *Bioconjug. Chem.* **27** 404–13

[50] Srivastava P, Verma V K and Sabbarwal S soluble metallic magnesium nanoclusters for bioimaging applications

[51] Kumar Verma V, Srivastava P, Sabbarwal S, Singh M, Koch B and Kumar M 2022

White Light Emitting Gadolinium Oxide Nanoclusters for In-vitro Bio-imaging *ChemistrySelect* **7**

[52] Sabbarwal S, Dubey A K, Pandey M and Kumar M 2020 Synthesis of biocompatible, BSA capped fluorescent CaCO3pre-nucleation nanoclusters for cell imaging applications *J. Mater. Chem. B* **8** 5729–44

[53] Zhu C, Chen Z, Gao S, Goh B L, Samsudin I Bin, Lwe K W, Wu Y, Wu C and Su X 2019 Recent advances in non-toxic quantum dots and their biomedical applications *Prog. Nat. Sci. Mater. Int.* **29** 628–40

[54] Mohammadi R, Naderi-Manesh H, Farzin L, Vaezi Z, Ayarri N, Samandari L and Shamsipur M 2022 Fluorescence sensing and imaging with carbon-based quantum dots for early diagnosis of cancer: A review *J. Pharm. Biomed. Anal.* **212** 114628

[55] Feng X and Zhang Y 2019 A simple and green synthesis of carbon quantum dots from coke for white light-emitting devices *RSC Adv.* **9** 33789–93

[56] Sowmiya P, Dhas T S, Inbakandan D, Anandakumar N, Nalini S, Suganya K S U, Remya R R, Karthick V and Kumar C M V 2023 Optically active organic and inorganic nanomaterials for biological imaging applications: A review *Micron* **172** 103486

[57] Chen L L, Zhao L, Wang Z G, Liu S L and Pang D W 2022 Near-Infrared-II Quantum Dots for In Vivo Imaging and Cancer Therapy *Small* **18**

[58] Rampazzo E, Genovese D, Palomba F, Prodi L and Zaccheroni N 2018 NIR-fluorescent dye doped silica nanoparticles for in vivo imaging, sensing and theranostic *Methods Appl. Fluoresc.* **6**

[59] Montalti M, Prodi L, Rampazzo E and Zaccheroni N 2014 Dye-doped silica

nanoparticles as luminescent organized systems for nanomedicine *Chem. Soc. Rev.* **43** 4243–68

[60] Lee J E, Lee N, Kim H, Kim J, Choi S H, Kim J H, Kim T, Song I C, Park S P, Moon W K and Hyeon T 2010 Uniform mesoporous dye-doped silica nanoparticles decorated with multiple magnetite nanocrystals for simultaneous enhanced magnetic resonance imaging, fluorescence imaging, and drug delivery *J. Am. Chem. Soc.* **132** 552–7

[61] Yang H, Akinoglu E M, Lisi F, Wu L, Shen S, Jin M, Zhou G, Giersig M, Shui L and Mulvaney P 2022 A versatile strategy for loading silica particles with dyes and quantum dots *Colloids Interface Sci. Commun.* **47** 100594

[62] MMR 2023 Phenolic antioxidant market - Global industry analysis and forecast (2023 - 2029) *Maximize Mark. Res.*

[63] Lifante J, Shen Y, Ximendes E, Martín Rodríguez E and Ortgies D H 2020 The role of tissue fluorescence in in vivo optical bioimaging *J. Appl. Phys.* **128**

[64] Wallyn J, Anton N, Akram S and Vandamme T F 2019 Biomedical Imaging: Principles, Technologies, Clinical Aspects, Contrast Agents, Limitations and Future Trends in Nanomedicines *Pharm. Res.* **36**

[65] Prabhakar N and Rosenholm J M 2019 Nanodiamonds for advanced optical bioimaging and beyond *Curr. Opin. Colloid Interface Sci.* **39** 220–31

[66] Wang J, Xu M, Wang D, Li Z, Primo F L, Tedesco A C and Bi H 2019 Copper-Doped Carbon Dots for Optical Bioimaging and Photodynamic Therapy *Inorg. Chem.* **58** 13394–402

[67] Pathania D, Sharma M, Sonu, Kumar S, Thakur P, Torino E, Janas D and Thakur S

2021 Essential oil derived biosynthesis of metallic nano-particles: Implementations above essence *Sustain. Mater. Technol.* **30** e00352

[68] Markowicz A 2023 The significance of metallic nanoparticles in the emerging, development and spread of antibiotic resistance *Sci. Total Environ.* **871** 162029

[69] Singh A, Gautam P K, Verma A, Singh V, Shivapriya P M, Shivalkar S, Sahoo A K and Samanta S K 2020 Green synthesis of metallic nanoparticles as effective alternatives to treat antibiotics resistant bacterial infections: A review *Biotechnol. Reports* **25** e00427

[70] Nejati M, Rostami M, Mirzaei H, Rahimi-Nasrabadi M, Vosoughifar M, Nasab A S and Ganjali M R 2022 Green methods for the preparation of MgO nanomaterials and their drug delivery, anti-cancer and anti-bacterial potentials: A review *Inorg. Chem. Commun.* **136** 109107

[71] Singh A, Amod A, Pandey P, Bose P, Pingali M S, Shivalkar S, Varadwaj P K, Sahoo A K and Samanta S K 2022 Bacterial biofilm infections, their resistance to antibiotics therapy and current treatment strategies *Biomed. Mater.* **17**

[72] Hadrup N, Sharma A K and Loeschner K 2018 Toxicity of silver ions, metallic silver, and silver nanoparticle materials after in vivo dermal and mucosal surface exposure: A review *Regul. Toxicol. Pharmacol.* **98** 257–67

[73] Nešporová K, Pavlík V, Šafránková B, Vágnerová H, Odráška P, Žídek O, Císařová N, Skoroplyas S, Kubala L and Velebný V 2020 Effects of wound dressings containing silver on skin and immune cells *Sci. Rep.* **10** 1–14

[74] Pathania D, Kumar S, Thakur P, Chaudhary V, Kaushik A, Varma R S, Furukawa H, Sharma M and Khosla A 2022 Essential oil-mediated biocompatible magnesium

nanoparticles with enhanced antibacterial, antifungal, and photocatalytic efficacies *Sci. Rep.* **12** 1–13

[75] Yin J, Hu Y and Yoon J 2015 Fluorescent probes and bioimaging: Alkali metals, alkaline earth metals and pH *Chem. Soc. Rev.* **44** 4619–44

[76] Weng Y, Jian Y, Huang W, Xie Z, Zhou Y and Pei X 2023 Alkaline earth metals for osteogenic scaffolds: From mechanisms to applications *J. Biomed. Mater. Res. - Part B Appl. Biomater.* **111** 1447–74

[77] Glasdam S M, Glasdam S and Peters G H 2016 The Importance of Magnesium in the Human Body: A Systematic Literature Review *Adv. Clin. Chem.* **73** 169–93

[78] Budnicka M, Sobiech M, Kolmas J and Luliński P 2022 Frontiers in ion imprinting of alkali- and alkaline-earth metal ions – Recent advancements and application to environmental, food and biomedical analysis *TrAC - Trends Anal. Chem.* **156**

[79] Moharramnejad M, Ehsani A, Shahi M, Gharanli S, Saremi H, Malekshah R E, Basmenj Z S, Salmani S and Mohammadi M 2023 MOF as nanoscale drug delivery devices: Synthesis and recent progress in biomedical applications *J. Drug Deliv. Sci. Technol.* **81** 104285

[80] Amukarimi S and Mozafari M 2021 Biodegradable magnesium-based biomaterials: An overview of challenges and opportunities *MedComm* **2** 123–44

[81] Zhang T, Wang W, Liu J, Wang L, Tang Y and Wang K 2022 A review on magnesium alloys for biomedical applications *Front. Bioeng. Biotechnol.* **10** 1–25

[82] Li J, Khalid A, Verma R, Abraham A, Qazi F, Dong X, Liang G and Tomljenovic-hanic S 2021 Silk fibroin coated magnesium oxide nanospheres: A biocompatible and biodegradable tool for noninvasive bioimaging applications *Nanomaterials* **11**

1–21

[83] Ali M, Hussein M A and Al-Aqeeli N 2019 Magnesium-based composites and alloys for medical applications: A review of mechanical and corrosion properties *J. Alloys Compd.* **792** 1162–90

[84] Gu X, Li Y, Qi C and Cai K 2022 Biodegradable magnesium phosphates in biomedical applications *J. Mater. Chem. B* **10** 2097–112

[85] Pandya A, Tripathi A, Purohit R, Singh S, Nandasiri M I, Karakoti A, Singh S P and Shanker R 2015 Fluorescent magnesium nanocomplex in a protein scaffold for cell nuclei imaging applications *RSC Adv.* **5** 94236–40

[86] Khalid A, Norello R, Abraham A N, Tetienne J P, Karle T J, Lui E W C, Xia K, Tran P A, O'Connor A J, Mann B G, De Boer R, He Y, Ng A M C, Djurisic A B, Shukla R and Tomljenovic-Hanic S 2019 Biocompatible and biodegradable magnesium oxide nanoparticles with in vitro photostable near-infrared emission: Short-term fluorescent markers *Nanomaterials* **9**

[87] Yan W, Zhang J, Abbas M, Li Y, Hussain S Z, Mumtaz S, Song Z, Hussain I and Tan B 2020 Facile synthesis of ultrastable fluorescent copper nanoclusters and their cellular imaging application *Nanomaterials* **10** 1–12

[88] Lin C-A J, Lee C-H, Hsieh J-T, Wang H-H, Li J K, Shen J-L, Chan W-H, Yeh H-I and Chang W H *Synthesis of Fluorescent Metallic Nanoclusters toward Biomedical Application: Recent Progress and Present Challenges* vol 29

[89] Duan X and Liu N 2019 Magnesium for Dynamic Nanoplasmonics *Acc. Chem. Res.* **52** 1979–89

[90] Liu Y, Lu B and Cai Z 2019 Recent Progress on Mg- And Zn-Based Alloys for

Biodegradable Vascular Stent Applications *J. Nanomater.* **2019**

[91] Pogorielov M, Husak E, Solodivnik A and Zhdanov S 2017 Magnesium-based biodegradable alloys: Degradation, application, and alloying elements *Interv. Med. Appl. Sci.* **9** 27–38

[92] Jebur Q M, Hashim A and Habeeb M A 2019 Structural, Electrical and Optical Properties for (Polyvinyl Alcohol–Polyethylene Oxide–Magnesium Oxide) Nanocomposites for Optoelectronics Applications *Trans. Electr. Electron. Mater.* **20** 334–43

[93] Shekhar S, Mahato P, Yadav R, Verma S D and Mukherjee S 2022 White Light Generation through l -Ascorbic Acid-Templated Thermoresponsive Copper Nanoclusters *ACS Sustain. Chem. Eng.* **10** 1379–89

[94] Sezer N, Evis Z, Kayhan S M, Tahmasebifar A and Koç M 2018 Review of magnesium-based biomaterials and their applications *J. Magnes. Alloy.* **6** 23–43

[95] Dong J, Lin T, Shao H, Wang H, Wang X, Song K and Li Q 2022 Advances in degradation behavior of biomedical magnesium alloys: A review *J. Alloys Compd.* **908** 164600

[96] Jahani B, Meesterb K, Wanga X and Brooks A 2020 Biodegradable Magnesium-Based Alloys for Bone Repair Applications: Prospects and challenges *Biomed Sci Instrum* **56** 292–304

[97] Zoroddu M A, Aaseth J, Crisponi G, Medici S, Peana M and Nurchi V M 2019 The essential metals for humans: a brief overview *J. Inorg. Biochem.* **195** 120–9

[98] Keerthiga N, Anitha R, Rajeshkumar S and Lakshmi T 2019 Antioxidant activity of cumin oil mediated silver nanoparticles *Pharmacogn. J.* **11** 787–9

[99] Sani A, Cao C and Cui D 2021 Toxicity of gold nanoparticles (AuNPs): A review *Biochem. Biophys. Reports* **26** 100991

[100] Zhang X D, Wu D, Shen X, Liu P X, Fan F Y and Fan S J 2012 In vivo renal clearance, biodistribution, toxicity of gold nanoclusters *Biomaterials* **33** 4628–38

[101] Carnovale C, Bryant G, Shukla R and Bansal V 2019 Identifying Trends in Gold Nanoparticle Toxicity and Uptake: Size, Shape, Capping Ligand, and Biological Corona *ACS Omega* **4** 242–56

[102] Alkilany A M and Murphy C J 2010 Toxicity and cellular uptake of gold nanoparticles: What we have learned so far? *J. Nanoparticle Res.* **12** 2313–33

[103] Demir E, Qin T, Li Y, Zhang Y, Guo X, Ingle T, Yan J, Orza A I, Biris A S, Ghorai S, Zhou T and Chen T 2020 Cytotoxicity and genotoxicity of cadmium oxide nanoparticles evaluated using in vitro assays *Mutat. Res. - Genet. Toxicol. Environ. Mutagen.* **850**–**851** 503149

[104] Jaishankar M, Tseten T, Anbalagan N, Mathew B B and Beeregowda K N 2014 Toxicity, mechanism and health effects of some heavy metals *Interdiscip. Toxicol.* **7** 60–72

[105] O'Brien T, Xu J and Patierno S R 2001 Effects of glutathione on chromium-induced DNA crosslinking and DNA polymerase arrest *Mol. Cell. Biochem.* **222** 173–82

[106] Ogunyemi S O, Zhang F, Abdallah Y, Zhang M, Wang Y, Sun G, Qiu W and Li B 2019 Biosynthesis and characterization of magnesium oxide and manganese dioxide nanoparticles using Matricaria chamomilla L. extract and its inhibitory effect on Acidovorax oryzae strain RS-2 *Artif. Cells, Nanomedicine Biotechnol.* **47** 2230–9

[107] Shin C H, Lee H Y, Gyan-Barimah C, Yu J H and Yu J S 2023 Magnesium:

properties and rich chemistry for new material synthesis and energy applications *Chem. Soc. Rev.* 2145–92

[108] Dutta S, Gupta S and Roy M 2020 Recent Developments in Magnesium Metal-Matrix Composites for Biomedical Applications: A Review *ACS Biomater. Sci. Eng.* **6** 4748–73

[109] Banjanin N and Belojevic G 2018 Changes of blood pressure and hemodynamic parameters after oral magnesium supplementation in patients with essential hypertension—an intervention study *Nutrients* **10** 8–14

[110] Wang L, Lu W, Qin J, Zhang F and Zhang D 2008 Microstructure and mechanical properties of cold-rolled TiNbTaZr biomedical β titanium alloy *Mater. Sci. Eng. A* **490** 421–6

[111] O'Neill E, Awale G, Daneshmandi L, Umerah O and Lo K W H 2018 The roles of ions on bone regeneration *Drug Discov. Today* **23** 879–90

[112] Zhou H, Liang B, Jiang H, Deng Z and Yu K 2021 Magnesium-based biomaterials as emerging agents for bone repair and regeneration: from mechanism to application *J. Magnes. Alloy.* **9** 779–804

[113] Haas I and Gedanken A 2008 Synthesis of metallic magnesium nanoparticles by sonoelectrochemistry *Chem. Commun.* 1795–7

[114] Kalidindi S B and Jagirdar B R 2009 Highly monodisperse colloidal magnesium nanoparticles by room temperature digestive ripening *Inorg. Chem.* **48** 4524–9

[115] Kooi B J, Palasantzas G and De Hosson J T M 2006 Gas-phase synthesis of magnesium nanoparticles: A high-resolution transmission electron microscopy study *Appl. Phys. Lett.* **89**

[116] Sergeev G B 2003 Cryochemistry of metal nanoparticles *J. Nanoparticle Res.* **5** 529–37

[117] Aurbach D, Lu Z, Schechter A, Gofer Y, Gizbar H, Turgeman R, Cohen Y, Moshkovich M and Levi E 2010 ChemInform Abstract: Prototype Systems for Rechargeable Magnesium Batteries. *ChemInform* **32** no-no

[118] Teunis M B, Lawrence K N, Dutta P, Siegel A P and Sardar R 2016 Pure white-light emitting ultrasmall organic-inorganic hybrid perovskite nanoclusters *Nanoscale* **8** 17433–9

[119] Muhamad Sarih N, Myers P, Slater A, Slater B, Abdullah Z, Tajuddin H A and Maher S 2019 White Light Emission from a Simple Mixture of Fluorescent Organic Compounds *Sci. Rep.* **9** 1–8

[120] Wang X Y, Hu Y X, Yang X F, Yin J, Chen Z and Liu S H 2019 Excitation Wavelength-Dependent Nearly Pure White Light-Emitting Crystals from a Single Gold(I)-Containing Complex *Org. Lett.* **21** 9945–9

[121] Khatun E, Bose S, Jash M and Pradeep T 2018 Atomically precise cluster-based white light emitters § *J. Chem. Sci.* **130** 1–9

[122] Anand U, Ghosh S and Mukherjee S 2012 Toggling between blue- and red-emitting fluorescent silver nanoclusters *J. Phys. Chem. Lett.* **3** 3605–9

[123] Díez I, Kanyuk M I, Demchenko A P, Walther A, Jiang H, Ikkala O and Ras R H A 2012 Blue, green and red emissive silver nanoclusters formed in organic solvents *Nanoscale* **4** 4434–7

[124] Bhandari S, Pramanik S, Khandelia R and Chattopadhyay A 2016 Gold Nanocluster and Quantum Dot Complex in Protein for Biofriendly White-Light-Emitting

Material *ACS Appl. Mater. Interfaces* **8** 1600–5

[125] Goswami U, Basu S, Paul A, Ghosh S S and Chattopadhyay A 2017 White light emission from gold nanoclusters embedded bacteria *J. Mater. Chem. C* **5** 12360–4

[126] Moreaud L, Prasad J, Mazères S, Marcelot C, Comby-Zerbino C, Antoine R, Heintz O and Dujardin E 2022 Facile one-pot synthesis of white emitting gold nanocluster solutions composed of red, green and blue emitters *J. Mater. Chem. C* **10** 2263–70

[127] Chithrani B D, Ghazani A A and Chan W C W 2006 Determining the size and shape dependence of gold nanoparticle uptake into mammalian cells *Nano Lett.* **6** 662–8

[128] Helmlinger J, Sengstock C, Groß-Heitfeld C, Mayer C, Schildhauer T A, Köller M and Epple M 2016 Silver nanoparticles with different size and shape: Equal cytotoxicity, but different antibacterial effects *RSC Adv.* **6** 18490–501

[129] Sangaiya P and Jayaprakash R 2018 A Review on Iron Oxide Nanoparticles and Their Biomedical Applications *J. Supercond. Nov. Magn.* **31** 3397–413

[130] Elahi B, Mirzaee M, Darroudi M, Kazemi Oskuee R, Sadri K and Amiri M S 2019 Preparation of cerium oxide nanoparticles in Salvia Macrosiphon Boiss seeds extract and investigation of their photo-catalytic activities *Ceram. Int.* **45** 4790–7

[131] Leng L, Xiong Q, Yang L, Li H, Zhou Y, Zhang W, Jiang S, Li H and Huang H 2021 An overview on engineering the surface area and porosity of biochar *Sci. Total Environ.* **763** 144204

[132] Nguyen D T C, Tran T Van, Kumar P S, Din A T M, Jalil A A and Vo D V N 2022 *Invasive plants as biosorbents for environmental remediation: a review* vol 20 (Springer International Publishing)

[133] Gozzi D, Tomellini M, Lazzarini L and Latini A 2010 High-temperature

determination of surface free energy of copper nanoparticles *J. Phys. Chem. C* **114** 12117–24

[134] Singh S, Prasad Chakraborty J and Kumar Mondal M 2020 Intrinsic kinetics, thermodynamic parameters and reaction mechanism of non-isothermal degradation of torrefied Acacia nilotica using isoconversional methods *Fuel* **259** 116263

[135] Singh B, Singh S and Kumar P 2021 In-depth analyses of kinetics, thermodynamics and solid reaction mechanism for pyrolysis of hazardous petroleum sludge based on isoconversional models for its energy potential *Process Saf. Environ. Prot.* **146** 85–94

[136] Li Q and Jun Y S 2018 The apparent activation energy and pre-exponential kinetic factor for heterogeneous calcium carbonate nucleation on quartz *Commun. Chem.* **1** 1–9

[137] Kumar M, Sabbarwal S, Mishra P K and Upadhyay S N 2019 Thermal degradation kinetics of sugarcane leaves (Saccharum officinarum L) using thermo-gravimetric and differential scanning calorimetric studies *Bioresour. Technol.* **279** 262–70

[138] Henrique M A, Flauzino Neto W P, Silvério H A, Martins D F, Gurgel L V A, Barud H da S, Morais L C de and Pasquini D 2015 Kinetic study of the thermal decomposition of cellulose nanocrystals with different polymorphs, cellulose I and II, extracted from different sources and using different types of acids *Ind. Crops Prod.* **76** 128–40

[139] Nawaz A, Mishra R K, Sabbarwal S and Kumar P 2021 Studies of physicochemical characterization and pyrolysis behavior of low-value waste biomass using Thermogravimetric analyzer: evaluation of kinetic and thermodynamic parameters *Bioresour. Technol. Reports* **16** 100858

[140] Wanjun T, Cunxin W and Donghua C 2006 An investigation of the pyrolysis kinetics of some aliphatic amino acids *J. Anal. Appl. Pyrolysis* **75** 49–53

[141] Starink M J 2003 The determination of activation energy from linear heating rate experiments: A comparison of the accuracy of isoconversion methods *Thermochim. Acta* **404** 163–76

[142] Dhyani V, Kumar J and Bhaskar T 2017 Thermal decomposition kinetics of sorghum straw via thermogravimetric analysis *Bioresour. Technol.* **245** 1122–9

[143] Vyazovkin S 2001 Modification of the Integral Isoconversional Method to Account for Variation in the Activation Energy *J. Comput. Chem.* **22** 178–83

[144] Vyazovkin S 1997 Advanced isoconversional method *J. Therm. Anal.* **49** 1493–9

[145] Bhakta R K, Maharrey S, Stavila V, Highley A, Alam T, Majzoub E and Allendorf M 2012 Thermodynamics and kinetics of NaAlH 4 nanocluster decomposition *Phys. Chem. Chem. Phys.* **14** 8160–9

[146] Joop H and Sefcik J 2020 *The Handbook of Continuous Crystallization* (The Royal Society of Chemistry)

[147] Hamm L M, Giuffre A J, Han N, Tao J, Wang D, De Yoreo J J and Dove P M 2014 Reconciling disparate views of template-directed nucleation through measurement of calcite nucleation kinetics and binding energies *Proc. Natl. Acad. Sci. U. S. A.* **111** 1304–9

[148] Wallace A F, DeYoreo J J and Dove P M 2009 Kinetics of silica nucleation on carboxyl- and amine-terminated surfaces: Insights for biomineralization *J. Am. Chem. Soc.* **131** 5244–50

[149] Chkonia G, Wölk J, Strey R, Wedekind J and Reguera D 2009 Evaluating nucleation

rates in direct simulations *J. Chem. Phys.* **130**

[150] Zhu Y, Li Q, Kim D, Min Y, Lee B and Jun Y S 2021 Sulfate-Controlled Heterogeneous CaCO3Nucleation and Its Non-linear Interfacial Energy Evolution *Environ. Sci. Technol.* **55** 11455–64

[151] Pitto-Barry A and Barry N P E 2019 Effect of Temperature on the Nucleation and Growth of Precious Metal Nanocrystals *Angew. Chemie - Int. Ed.* **58** 18482–6

[152] Oyelaran O, Novet T, Johnson C D and Johnson D C 1996 Controlling solid-state reaction pathways: Composition dependence in the nucleation energy of InSe *J. Am. Chem. Soc.* **118** 2422–6

[153] Cai L, Chen J, Liu Z, Wang H, Yang H and Ding W 2018 Magnesium oxide nanoparticles: Effective agricultural antibacterial agent against Ralstonia solanacearum *Front. Microbiol.* **9** 1–19

[154] Sabbagh F and Muhamad I I 2017 Acrylamide-based hydrogel drug delivery systems: Release of Acyclovir from MgO nanocomposite hydrogel *J. Taiwan Inst. Chem. Eng.* **72** 182–93

[155] Younis I Y, El-Hawary S S, Eldahshan O A, Abdel-Aziz M M and Ali Z Y 2021 Green synthesis of magnesium nanoparticles mediated from Rosa floribunda charisma extract and its antioxidant, antiaging and antibiofilm activities *Sci. Rep.* **11** 1–15

[156] Saied E, Eid A M, Hassan S E, Salem S S, Radwan A A, Halawa M, Saleh F M, Saad H A, Saied E M and Fouda A 2021 The Catalytic Activity of Biosynthesized Magnesium Oxide Chromium Ion Removal *Catalysts* **11** 1–21

[157] Fernandez M, RB Singh K, Sarkar T, Singh P and Pratap Singh R 2020 Aplicaciones

recientes de nanopartículas de óxido de magnesio (MgO) en varios dominios *Adv. Mater. Lett.*

[158] Nagai N, Iwai Y, Deguchi S, Otake H, Kanai K, Okamoto N and Shimomura Y 2019 Therapeutic potential of a combination of magnesium hydroxide nanoparticles and sericin for epithelial corneal wound healing *Nanomaterials* **9**

[159] Yin M, Wu J, Deng M, Wang P, Ji G, Wang M, Zhou C, Blum N T, Zhang W, Shi H, Jia N, Wang X and Huang P 2021 Multifunctional Magnesium Organic Framework-Based Microneedle Patch for Accelerating Diabetic Wound Healing *ACS Nano* **15** 17842–53

[160] Anon Microbiology and Immunology - 2018 - Hayat - In vitro antibiofilm and anti-adhesion effects of magnesium oxide.pdf

[161] De Silva R T, Mantilaka M M M G P G, Goh K L, Ratnayake S P, Amaratunga G A J and De Silva K M N 2017 Magnesium Oxide Nanoparticles Reinforced Electrospun Alginate-Based Nanofibrous Scaffolds with Improved Physical Properties *Int. J. Biomater.* **2017**

[162] Liu M, Wang R, Liu J, Zhang W, Liu Z, Lou X, Nie H, Wang H, Mo X, Abd-Elhamid A I, Zheng R and Wu J 2022 Incorporation of magnesium oxide nanoparticles into electrospun membranes improves pro-angiogenic activity and promotes diabetic wound healing *Biomater. Adv.* **133** 112609

[163] Liu M, Wang X, Li H, Xia C, Liu Z, Liu J, Yin A, Lou X, Wang H, Mo X and Wu J 2021 Magnesium oxide-incorporated electrospun membranes inhibit bacterial infections and promote the healing process of infected wounds *J. Mater. Chem. B* **9** 3727–44

[164] Khalajabadi S Z, Abu A B H, Ahmad N, Kadir M R A, Ismail A F, Nasiri R, Haider W and Redzuan N B H 2017 Biodegradable Mg/HA/TiO 2 nanocomposites coated with MgO and Si/MgO for orthopedic applications: A study on the corrosion, surface characterization, and biocompatability *Coatings* **7**

[165] Li Y, Feng L, Yan W, Hussain I, Su L and Tan B 2019 PVP-templated highly luminescent copper nanoclusters for sensing trinitrophenol and living cell imaging *Nanoscale* **11** 1286–94

[166] Zhang Q, Yang M, Zhu Y and Mao C 2017 Metallic Nanoclusters for Cancer Imaging and Therapy *Curr. Med. Chem.* **25** 1379–96

[167] Amina M, Al Musayeib N M, Alarfaj N A, El-Tohamy M F, Oraby H F, Al Hamoud G A, Bukhari S I and Moubayed N M S 2020 Biogenic green synthesis of MgO nanoparticles using Saussurea costus biomasses for a comprehensive detection of their antimicrobial, cytotoxicity against MCF-7 breast cancer cells and photocatalysis potentials *PLoS One* **15** 1–23

[168] Zhou Z Y, Tian N, Li J T, Broadwell I and Sun S G 2011 Nanomaterials of high surface energy with exceptional properties in catalysis and energy storage *Chem. Soc. Rev.* **40** 4167–85

[169] Sarparast M, Noori A, Ilkhani H, Bathaie S Z, El-Kady M F, Wang L J, Pham H, Marsh K L, Kaner R B and Mousavi M F 2016 Cadmium nanoclusters in a protein matrix: Synthesis, characterization, and application in targeted drug delivery and cellular imaging *Nano Res.* **9** 3229–46

[170] Malik K A, Malik J H, Bhat A A, Assadullah I and Tomar R 2021 Trap assisted visible light luminescent properties of hydrothermally grown Gd doped ZnO nanostructures *Vacuum* **183** 109832

[171] Xie J, Zheng Y and Ying J Y 2009 Protein-directed synthesis of highly fluorescent gold nanoclusters *J. Am. Chem. Soc.* **131** 888–9

[172] Pennycook T J, McBride J R, Rosenthal S J, Pennycook S J and Pantelides S T 2012 Dynamic fluctuations in ultrasmall nanocrystals induce white light emission *Nano Lett.* **12** 3038–42

[173] Zhang Y, Zhang C, Xu C, Wang X, Liu C, Waterhouse G I N, Wang Y and Yin H 2019 Ultrasmall Au nanoclusters for biomedical and biosensing applications: A mini-review *Talanta* **200** 432–42

[174] Goswami N, Giri A, Bootharaju M S, Xavier P L, Pradeep T and Pal S K 2011 Copper quantum clusters in protein matrix: Potential sensor of Pb 2+ ion *Anal. Chem.* **83** 9676–80

[175] Cai Z, Li H, Wu J, Zhu L, Ma X and Zhang C 2020 Ascorbic acid stabilised copper nanoclusters as fluorescent sensors for detection of quercetin *RSC Adv.* **10** 8989–93

[176] Xu Y, Sherwood J, Qin Y, Crowley D, Bonizzoni M and Bao Y 2014 The role of protein characteristics in the formation and fluorescence of Au nanoclusters *Nanoscale* **6** 1515–24

[177] Chen S, Zhao X, Wang Y, Shi J and Liu D 2012 White light emission with red-green-blue lasing action in a disordered system of nanoparticles *Appl. Phys. Lett.* **101**

[178] Tanwar S, Sharma B, Kaur V and Sen T 2019 White light emission from a mixture of silicon quantum dots and gold nanoclusters and its utilities in sensing of mercury(ii) ions and thiol containing amino acid *RSC Adv.* **9** 15997–6006

[179] Yuan T, Yuan F, Li X, Li Y, Fan L and Yang S 2019 Fluorescence-phosphorescence

dual emissive carbon nitride quantum dots show 25% white emission efficiency enabling single-component WLEDs *Chem. Sci.* **10** 9801–6

[180] Nelli I, Kaczmarek A M, Locardi F, Caratto V, Costa G A and Van Deun R 2017 Multidoped Ln3+ gadolinium dioxycarbonates as tunable white light emitting phosphors *Dalt. Trans.* **46** 2785–92

[181] Wu Z F, Tan B, Wang J Y, Du C F, Deng Z H and Huang X Y 2015 Tunable photoluminescence and direct white-light emission in Mg-based coordination networks *Chem. Commun.* **51** 157–60

[182] Sreeja V, Jayaprabha K N and Joy P A 2015 Water-dispersible ascorbic-acid-coated magnetite nanoparticles for contrast enhancement in MRI *Appl. Nanosci.* **5** 435–41

[183] Sabbarwal S, Dubey A K, Pandey M and Kumar M 2020 Synthesis of biocompatible, BSA capped fluorescent CaCO3pre-nucleation nanoclusters for cell imaging applications *J. Mater. Chem. B* **8** 5729–44

[184] Mordike B L and Ebert T 2001 Magnesium Properties - applications - potential *Mater. Sci. Eng. A* **302** 37–45

[185] Geiger H and Wanner C 2012 Magnesium in disease *CKJ Clin. Kidney J.* **5**

[186] Yartys V A, Lototskyy M V., Akiba E, Albert R, Antonov V E, Ares J R, Baricco M, Bourgeois N, Buckley C E, Bellosta von Colbe J M, Crivello J C, Cuevas F, Denys R V., Dornheim M, Felderhoff M, Grant D M, Hauback B C, Humphries T D, Jacob I, Jensen T R, de Jongh P E, Joubert J M, Kuzovnikov M A, Latroche M, Paskevicius M, Pasquini L, Popilevsky L, Skripnyuk V M, Rabkin E, Sofianos M V., Stuart A, Walker G, Wang H, Webb C J and Zhu M 2019 Magnesium based materials for hydrogen based energy storage: Past, present and future *Int. J.*

Hydrogen Energy **44** 7809–59

[187] Peng Y, Wang P, Luo L, Liu L and Wang F 2018 Green synthesis of fluorescent palladium nanoclusters *Materials (Basel).* **11**

[188] Qu X, Li Y, Li L, Wang Y, Liang J and Liang J 2015 Fluorescent gold nanoclusters: Synthesis and recent biological application *J. Nanomater.* **2015**

[189] Sood A, Arora V, Shah J, Kotnala R K and Jain T K 2016 Ascorbic acid-mediated synthesis and characterisation of iron oxide/gold core–shell nanoparticles. *J. Exp. Nanosci.* **11** 370–82

[190] Xu N, Li H W, Yue Y and Wu Y 2016 Synthesis of bovine serum albumin-protected high fluorescence Pt16-nanoclusters and their application to detect sulfide ions in solutions *Nanotechnology* **27**

[191] Yokoi T and Ishii K 2018 Dependence of phthalocyanine-based fluorescence on albumin structure: A fluorescent probe for ascorbic acid *J. Photochem. Photobiol. A Chem.* **364** 1–5

[192] Wang X, Liu Z, Zhao W, Sun J, Qian B, Wang X, Zeng H, Du D and Duan J 2019 A novel switchable fluorescent sensor for facile and highly sensitive detection of alkaline phosphatase activity in a water environment with gold/silver nanoclusters *Anal. Bioanal. Chem.* **411** 1009–17

[193] Narayan S, Rajagopalan A, Reddy J S and Chadha A 2014 BSA binding to silica capped gold nanostructures: Effect of surface cap and conjugation design on nanostructure-BSA interface *RSC Adv.* **4** 1412–20

[194] Coil I, Prepared H, Fluorescent H and Sensor E 2014 Electronic Supplementary Information Induction Coil Heater Prepared Highly Fluorescent Carbon Dots as

Invisible Ink and Explosive Sensor 1–14

[195] Sahoo A K, Banerjee S, Ghosh S S and Chattopadhyay A 2014 Simultaneous RGB emitting Au nanoclusters in chitosan nanoparticles for anticancer gene theranostics *ACS Appl. Mater. Interfaces* **6** 712–24

[196] Suo Z, Hou X, Liu Y, Xing F, Chen Y and Feng L 2020 β-Lactoglobulin amyloid fibril-templated gold nanoclusters for cellular multicolor fluorescence imaging and colorimetric blood glucose assay *Analyst* **145** 6919–27

[197] Ursache F M, Aprodu I, Nistor O V, Bratu M, Botez E and Stănciuc N 2017 Probing the heat-induced structural changes in bovine serum albumin by fluorescence spectroscopy and molecular modelling *Int. J. Dairy Technol.* **70** 424–31

[198] Wang P Y, Yang C T and Chu L K 2021 Differentiating the protein dynamics using fluorescence evolution of tryptophan residue(s): A comparative study of bovine and human serum albumins upon temperature jump *Chem. Phys. Lett.* **781** 138998

[199] Ghisaidoobe A B T and Chung S J 2014 Intrinsic tryptophan fluorescence in the detection and analysis of proteins: A focus on förster resonance energy transfer techniques *Int. J. Mol. Sci.* **15** 22518–38

[200] He P, Shi Y, Meng T, Yuan T, Li Y, Li X, Zhang Y, Fan L and Yang S 2020 Recent advances in white light-emitting diodes of carbon quantum dots *Nanoscale* **12** 4826–32

[201] Patel A S and Mohanty T 2014 Silver nanoclusters in BSA template: A selective sensor for hydrogen peroxide *J. Mater. Sci.* **49** 2136–43

[202] Lillo C R, Calienni M N, Rivas Aiello B, Prieto M J, Rodriguez Sartori D, Tuninetti J, Toledo P, Alonso S del V, Moya S, Gonzalez M C, Montanari J and Soler-Illia G

J A A 2020 BSA-capped gold nanoclusters as potential theragnostic for skin diseases: Photoactivation, skin penetration, in vitro, and in vivo toxicity *Mater. Sci. Eng. C* **112** 110891

[203] Li X, Wang G, Chen D and Lu Y 2014 Binding of ascorbic acid and α-tocopherol to bovine serum albumin: A comparative study *Mol. Biosyst.* **10** 326–37

[204] Dementjev A P, De Graaf A, Van de Sanden M C M, Maslakov K I, Naumkin A V. and Serov A A 2000 X-ray photoelectron spectroscopy reference data for identification of the C3N4 phase in carbon-nitrogen films *Diam. Relat. Mater.* **9** 1904–7

[205] Liu H, Yang J, Zhang Y, Yang L, Wei M and Ding X 2009 Structure and magnetic properties of Fe-doped ZnO prepared by the sol–gel method *J. Phys. Condens. Matter* **21** 145803

[206] Barr T L and Seal S 1995 Nature of the use of adventitious carbon as a binding energy standard *J. Vac. Sci. Technol. A Vacuum, Surfaces, Film.* **13** 1239–46

[207] Dobrovolsky V D, Khyzhun O Y, Sinelnichenko A K, Ershova O G and Solonin Y M 2017 XPS study of influence of exposure to air on thermal stability and kinetics of hydrogen decomposition of MgH2 films obtained by direct hydrogenation from gaseous phase of metallic ... Journal of Electron Spectroscopy and XPS study of influence of exposure *J. Electron Spectros. Relat. Phenomena* **215** 28–35

[208] Haider N C and Alonso J 1975 Valence and Core Electron Spectra of Mg in MgO in Evoporated Thin Films

[209] Talapatra A, Bandyopadhyay S K, Sen P, Barat P, Mukherjee S and Mukherjee M 2005 X-ray photoelectron spectroscopy studies of MgB2 for valence state of Mg

Phys. C Supercond. its Appl. **419** 141–7

[210] Tajima K, Yamada Y, Bao S, Okada M and Yoshimura K 2010 Characterization of flexible switchable mirror film prepared by DC magnetron sputtering *Vacuum* **84** 1460–5

[211] Tajima K, Hotta H, Yamada Y, Okada M and Yoshimura K 2012 Environmental durability of electrochromic switchable mirror glass at sub-zero temperature *Sol. Energy Mater. Sol. Cells* **104** 146–51

[212] Yeh Y Q, Liao K F, Shih O, Shiu Y J, Wu W R, Su C J, Lin P C and Jeng U S 2017 Probing the Acid-Induced Packing Structure Changes of the Molten Globule Domains of a Protein near Equilibrium Unfolding *J. Phys. Chem. Lett.* **8** 470–7

[213] El Kadi N, Taulier N, Le Huérou J Y, Gindre M, Urbach W, Nwigwe I, Kahn P C and Waks M 2006 Unfolding and refolding of bovine serum albumin at acid pH: Ultrasound and structural studies *Biophys. J.* **91** 3397–404

[214] Ren S, Deng L, Zhang B, Lei Y, Ren H, Lv J, Zhao R and Chen X 2019 Effect of air oxidation on texture, surface properties and dye adsorption of wood-derived porous carbon materials *Materials (Basel).* **12**

[215] Zhu M, Lan J, Zhang X, Sui G and Yang X 2017 Porous carbon derived from: Ailanthus altissima with unique honeycomb-like microstructure for high-performance supercapacitors *New J. Chem.* **41** 4281–5

[216] Online V A 2013 Highly conductive NiCo 2 S 4 urchin-like nanostructures for high-rate pseudocapacitors † 1–5

[217] Zhang Y, Zhang Y, Zhang Y, Si H and Sun L 2019 Bimetallic - NiCo 2 S 4 Nanoneedles Anchored on Mesocarbon Microbeads as Advanced Electrodes for

Asymmetric Supercapacitors *Nano-Micro Lett.* **11** 1–15

[218] Guével X Le, Spies C, Daum N, Jung G and Schneider M 2012 Highly Fluorescent Silver Nanoclusters Stabilized by Glutathione : A Promising Fluorescent Label for Bioimaging **5** 379–87

[219] Dainese T, Antonello S, Bogialli S, Fei W, Venzo A and Maran F 2018 Gold Fusion: From Au25(SR)18 to Au38(SR)24, the Most Unexpected Transformation of a Very Stable Nanocluster *ACS Nano* **12** 7057–66

[220] Ghosh R, Sahoo A K, Ghosh S S, Paul A and Chattopadhyay A 2014 Blue-emitting copper nanoclusters synthesized in the presence of lysozyme as candidates for cell labeling *ACS Appl. Mater. Interfaces* **6** 3822–8

[221] Xavier P L, Chaudhari K, Verma P K, Pal S K and Pradeep T 2010 Luminescent quantum clusters of gold in transferrin family protein, lactoferrin exhibiting FRET *Nanoscale* **2** 2769–76

[222] Alhazmi H A 2019 FT-IR spectroscopy for the identification of binding sites and measurements of the binding interactions of important metal ions with bovine serum albumin *Sci. Pharm.* **87**

[223] Vahdatkhah P, Madaah Hosseini H R, Khodaei A, Montazerabadi A R, Irajirad R, Oghabian M A and Delavari H. H 2015 Rapid microwave-assisted synthesis of PVP-coated ultrasmall gadolinium oxide nanoparticles for magnetic resonance imaging *Chem. Phys.* **453**–**454** 35–41

[224] Govindaraju S, Ankireddy S R, Viswanath B, Kim J and Yun K 2017 Fluorescent Gold Nanoclusters for Selective Detection of Dopamine in Cerebrospinal fluid *Sci. Rep.* **7**

[225] Sabaa M W, Hanna D H, Abu Elella M H and Mohamed R R 2019 Encapsulation of bovine serum albumin within novel xanthan gum based hydrogel for protein delivery *Mater. Sci. Eng. C* **94** 1044–55

[226] Paulo-Mirasol S, Martínez-Ferrero E and Palomares E 2019 Direct white light emission from carbon nanodots (C-dots) in solution processed light emitting diodes *Nanoscale* **11** 11315–21

[227] Yang T Q, Peng B, Shan B Q, Zong Y X, Jiang J G, Wu P and Zhang K 2020 Origin of the photoluminescence of metal nanoclusters: From metal-centered emission to ligand-centered emission *Nanomaterials* **10**

[228] Ran X, Ran X, Zhang Q, Zhang Y, Chen J, Wei Z, He Y, He Y, Guo L and Guo L 2020 Probing the electron transfer between iLOV protein and ag nanoparticles *Molecules* **25** 1–11

[229] Tairi L, Touam S, Boumaza A, Boukhtouta M, Meradji H, Ghemid S, Omran S Bin, Hassan F E H and Khenata R 2017 Phase stability and electronic behavior of MgS, MgSe and MgTe compounds *Phase Transitions* **90** 929–41

[230] Bhandari U, Ayirizia B A, Malozovsky Y, Franklin L and Bagayoko D 2020 First principle investigation of electronic, transport, and bulk properties of zinc-blende magnesium sulfide *Electron.* **9** 1–9

[231] Lany S 2014 Polymorphism, band-structure, band-lineup, and alloy energetics of the group II oxides and sulfides MgO, ZnO, CdO, MgS, ZnS, CdS *Oxide-based Mater. Devices V* **8987** 89870K

[232] Millican S L, Clary J M, Bartel C J, Singstock N R, Holder M and Musgrave C B Alloying behavior of wide band gap alkaline-earth chalcogenides

[233] Bhandari U, Bamba C O, Malozovsky Y, Franklin L S and Bagayoko D 2018 Predictions of Electronic, Transport, and Structural Properties of Magnesium Sulfide (MgS) in the Rocksalt Structure *J. Mod. Phys.* **09** 1773–84

[234] Zhao C, Duan Y, Gao J and Dong H 2017 Crystal and band structures of ZnS, MgS, and ZnS-MgS alloys *J. Appl. Phys.* **121**

[235] Chen X, Lv G, Zhang J, Tang S, Yan Y, Wu Z, Su J and Wei J 2014 Preparation and properties of bsa-loaded microspheres based on multi-(amino acid) copolymer for protein delivery *Int. J. Nanomedicine* **9** 1957–65

[236] Carpenter J E and Grünwald M 2021 Pre-Nucleation Clusters Predict Crystal Structures in Models of Chiral Molecules *J. Am. Chem. Soc.* **143** 21580–93

[237] Ray S, Bhattacharya T K, Singh V K, Deb D, Ghosh S and Das S 2021 Non-isothermal decomposition kinetics of nano-scale CaCO3 as a function of particle size variation *Ceram. Int.* **47** 858–64

[238] Wang C, Wang C, Xu L, Cheng H, Lin Q and Zhang C 2014 Protein-directed synthesis of pH-responsive red fluorescent copper nanoclusters and their applications in cellular imaging and catalysis *Nanoscale* **6** 1775–81

[239] Kannan V, Hazeli K and Ramesh K T 2018 The mechanics of dynamic twinning in single crystal magnesium *J. Mech. Phys. Solids* **120** 154–78

[240] Mooij L and Dam B 2013 Nucleation and growth mechanisms of nano magnesium hydride from the hydrogen sorption kinetics *Phys. Chem. Chem. Phys.* **15** 11501–10

[241] Zabihi O and Khodabandeh A 2013 Understanding of thermal/thermo-oxidative degradation kinetics of polythiophene nanoparticles *J. Therm. Anal. Calorim.* **112** 1507–13

[242] Ebrahimi-Kahrizsangi R and Abbasi M H 2008 Evaluation of reliability of Coats-Redfern method for kinetic analysis of non-isothermal TGA *Trans. Nonferrous Met. Soc. China (English Ed.* **18** 217–21

[243] Budrugeac P 2000 Evaluation of the non-isothermal kinetic parameters of the thermal and thermo-oxidative degradation of polymers and polymeric materials: Its use and abuse *Polym. Degrad. Stab.* **71** 185–7

[244] Budrugeac P 2005 Some methodological problems concerning the kinetic analysis of non-isothermal data for thermal and thermo-oxidative degradation of polymers and polymeric materials *Polym. Degrad. Stab.* **89** 265–73

[245] Kumar M, Srivastava N, Upadhyay S N and Mishra P K 2021 Thermal degradation of dry kitchen waste: kinetics and pyrolysis products *Biomass Convers. Biorefinery*

[246] Kissinger H E 1957 Reaction Kinetics in Differential Thermal Analysis *Anal. Chem.* **29** 1702–6

[247] Flynn J H 1997 The “temperature integral” - Its use and abuse *Thermochim. Acta* **300** 83–92

[248] Gajera B and Panwar N L 2019 Pyrolysis and kinetic behaviour of black gram straw using thermogravimetric analysis *Energy Sources, Part A Recover. Util. Environ. Eff.* **0** 1–14

[249] Mishra G and Bhaskar T 2014 Non isothermal model free kinetics for pyrolysis of rice straw *Bioresour. Technol.* **169** 614–21

[250] Senum G I and Yang R T 1977 Rational approximations of the integral of the Arrhenius function *J. Therm. Anal.* **11** 445–7

[251] Topală T, Bodoki A, Oprean L and Oprean R 2014 Bovine serum albumin

interactions with metal complexes *Clujul Med.* **87** 5

[252] Mérel P, Tabbal M, Chaker M, Moisa S and Margot J 1998 Direct evaluation of the sp 3 content in diamond-like-carbon films by XPS *Appl. Surf. Sci.* **136** 105–10

[253] Wu J B, Chang J J, Li M Y, Leu M S and Li A K 2007 Characterization of diamond-like carbon coatings prepared by pulsed bias cathodic vacuum arc deposition *Thin Solid Films* **516** 243–7

[254] Zhang C, Jin J, Zhao J, Jiang W and Yin J 2013 Functionalized polypropylene non-woven fabric membrane with bovine serum albumin and its hemocompatibility enhancement *Colloids Surfaces B Biointerfaces* **102** 45–52

[255] Nguyen T P, Amgaad K, Cailler M, Tran V H and Lefrant S 1995 XPS analysis of thermal and plasma treated polyparaphenylene-vinylene thin films and their interface formed with aluminum layer *Synth. Met.* **69** 495–6

[256] Ghodbane S, Ballutaud D, Omnès F and Agnès C 2010 Comparison of the XPS spectra from homoepitaxial {111}, {100} and polycrystalline boron-doped diamond films *Diam. Relat. Mater.* **19** 630–6

[257] Au C T and Roberts M W 1985 Structure of the chloride overlayer at a magnesium surface *Surf. Sci. Lett.* **149** 18–24

[258] Fuggle J C 1977 XPS, UPS AND XAES studies of oxygen adsorption on polycrystalline Mg at ~100 and ~300 K *Surf. Sci.* **69** 581–608

[259] Haider N C, Alonso J and Swartz W E 1975 Valence and Core Electron Spectra of Mg in MgO in Evoporated Thin Films *Zeitschrift fur Naturforsch.ung - Sect. A J. Phys. Sci.* **30** 1485–90

[260] Tajima K, Yamada Y and Yoshimura K 2014 Switchable mirror glass with a Mg-

Zr-Ni ternary alloy thin film *Sol. Energy Mater. Sol. Cells* **126** 227–36

[261] Fischer A, Köstler H and Schlapbach L 1991 Hydrogen in magnesium alloys and magnesium interfaces: preparation, electronic properties and interdiffusion *J. Less-Common Met.* **172**–**174** 808–15

[262] Yoshimura K, Yamada Y and Okada M 2004 Hydrogenation of Pd capped Mg thin films at room temperature *Surf. Sci.* **566**–**568** 751–4

[263] Zheng C, Wang H, Xu W, Xu C, Liang J and Han H 2014 Study on the interaction between histidine-capped Au nanoclusters and bovine serum albumin with spectroscopic techniques *Spectrochim. Acta - Part A Mol. Biomol. Spectrosc.* **118** 897–902

[264] Khawam A and Flanagan D R 2006 Solid-state kinetic models: Basics and mathematical fundamentals *J. Phys. Chem. B* **110** 17315–28

[265] Vyazovkin S, Burnham A K, Criado J M, Pérez-Maqueda L A, Popescu C and Sbirrazzuoli N 2011 ICTAC Kinetics Committee recommendations for performing kinetic computations on thermal analysis data *Thermochim. Acta* **520** 1–19

[266] Norberto D R, Vieira J M, de Souza A R, Bispo J A C and Bonafe C F S 2012 Pressure- and Urea-Induced Denaturation of Bovine Serum Albumin: Considerations about Protein Heterogeneity *Open J. Biophys.* **02** 4–14

[267] Merabia S, Shenogin S, Joly L, Keblinski P and Barrat J L 2009 Heat transfer from nanoparticles: A corresponding state analysis *Proc. Natl. Acad. Sci. U. S. A.* **106** 15113–8

[268] Evans T and Strezov L 2000 Interfacial heat transfer and nucleation of steel on metallic substrates *Metall. Mater. Trans. B Process Metall. Mater. Process. Sci.* **31**

1081–9

[269] Yuan X, He T, Cao H and Yuan Q 2017 Cattle manure pyrolysis process: Kinetic and thermodynamic analysis with isoconversional methods *Renew. Energy* **107** 489–96

[270] Palmay P, Mora M, Barzallo D and Bruno J C 2021 Determination of thermodynamic parameters of polylactic acid by thermogravimetry under pyrolysis conditions *Appl. Sci.* **11**

[271] Thomas J J 2007 A new approach to modeling the nucleation and growth kinetics of tricalcium silicate hydration *J. Am. Ceram. Soc.* **90** 3282–8

[272] Aashima, Pandey S K, Singh S and Mehta S K 2018 Biocompatible gadolinium oxide nanoparticles as efficient agent against pathogenic bacteria *J. Colloid Interface Sci.* **529** 496–504

[273] Wei H, Wang Z, Yang L, Tian S, Hou C and Lu Y 2010 Lysozyme-stabilized gold fluorescent cluster: Synthesis and application as Hg2+ sensor *Analyst* **135** 1406–10

[274] Pang S and Liu S 2017 Lysozyme-stabilized bimetallic gold/silver nanoclusters as a turn-on fluorescent probe for determination of ascorbic acid and acid phosphatase *Anal. Methods* **9** 6713–8

[275] Patel P, Parmar K, Patel D, Kumar S, Trivedi M and Das M 2018 Inhibition of amyloid fibril formation of lysozyme by ascorbic acid and a probable mechanism of action *Int. J. Biol. Macromol.* **114** 666–78

[276] Mo Q, Liu F, Gao J, Zhao M and Shao N 2018 Fluorescent sensing of ascorbic acid based on iodine induced oxidative etching and aggregation of lysozyme-templated silver nanoclusters *Anal. Chim. Acta* **1003** 49–55

[277] Anon ChemistrySelect - 2022 - Kumar Verma - White Light Emitting Gadolinium Oxide Nanoclusters for In-vitro Bio-imaging.pdf

[278] Muthu M S, Kutty R V, Luo Z, Xie J and Feng S S 2015 Theranostic vitamin E TPGS micelles of transferrin conjugation for targeted co-delivery of docetaxel and ultra bright gold nanoclusters *Biomaterials* **39** 234–48

[279] Das S, Goswami P, Verma V K, Indurthi H K, Kumar M, Koch B and Sharma D K 2023 Rapid access to 7-substituted cycloalkylamino and alkylamino analogues of 4-methylcoumarin reveals surprising emitters *Dye. Pigment.* **217** 111407

[280] Thawari A G, Kumar P, Srivastava R and Rao C P 2020 Lysozyme coated copper nanoclusters for green fluorescence and their utility in cell imaging *Mater. Adv.* **1** 1439–47

[281] Cao H, Cui T, Jin G and Liu X 2014 Cellular responses to titanium successively treated by magnesium and silver PIII&D *Surf. Coatings Technol.* **256** 9–14

[282] Buchner F, Forster-Tonigold K, Bolter T, Rampf A, Klein J, Groß A and Behm R J 2022 Interaction of Mg with the ionic liquid 1-butyl-1-methylpyrrolidinium bis(trifluoromethylsulfonyl)imide—An experimental and computational model study of the electrode–electrolyte interface in post-lithium batteries *J. Vac. Sci. Technol. A* **40** 023204

[283] Ag M 1983 Monochromatized Ag **5**

[284] Holen I, Speirs V, Morrissey B and Blyth K 2017 In vivo models in breast cancer research: Progress, challenges and future directions *DMM Dis. Model. Mech.* **10** 359–71

[285] Mittal A K, Chisti Y and Banerjee U C 2013 Synthesis of metallic nanoparticles

using plant extracts *Biotechnol. Adv.* **31** 346–56

[286] Vilas V, Philip D and Mathew J 2016 Essential oil mediated synthesis of silver nanocrystals for environmental, anti-microbial and antioxidant applications *Mater. Sci. Eng. C* **61** 429–36

[287] Sadiq M U, Shah A, Haleem A, Shah S M and Shah I 2023 Eucalyptus globulus Mediated Green Synthesis of Environmentally Benign Metal Based Nanostructures: A Review *Nanomaterials* **13**

[288] Ijaz I, Gilani E, Nazir A and Bukhari A 2020 Detail review on chemical, physical and green synthesis, classification, characterizations and applications of nanoparticles *Green Chem. Lett. Rev.* **13** 59–81

[289] Sana S S, Li H, Zhang Z, Sharma M, Usmani Z, Hou T, Netala V R, Wang X and Gupta V K 2021 Recent advances in essential oils-based metal nanoparticles: A review on recent developments and biopharmaceutical applications *J. Mol. Liq.* **333** 115951

[290] Obeizi Z, Benbouzid H, Ouchenane S, Yılmaz D, Culha M and Bououdina M 2020 Biosynthesis of Zinc oxide nanoparticles from essential oil of Eucalyptus globulus with antimicrobial and anti-biofilm activities *Mater. Today Commun.* **25**

[291] Surendra T V, Mohana Roopan S and Khan M R 2019 Biogenic approach to synthesize rod shaped Gd2O3 nanoparticles and its optimization using response surface methodology-Box–Behnken design model *Biotechnol. Prog.* **35** 1–12

[292] Gonfa Y H, Gelagle A A, Hailegnaw B, Kabeto S A, Workeneh G A, Tessema F B, Tadesse M G, Wabaidur S M, Dahlous K A, Abou Fayssal S, Kumar P, Adelodun B, Bachheti A and Bachheti R K 2023 Optimization, Characterization, and

Biological Applications of Silver Nanoparticles Synthesized Using Essential Oil of Aerial Part of Laggera tomentosa *Sustain.* **15**

[293] Qaralleh H, Khleifat K, Al-Limoun M, Al-Tarawneh A, Khleifat W, Almajali I, Buqain R, Shadid K A and Alsowayeh N 2022 Antibacterial activity of airborne fungal mediated nanoparticles in combination with Foeniculum vulgare essential oil *J. HerbMed Pharmacol.* **11** 419–27

[294] Verma A, Shivalkar S, Sk M P, Samanta S K and Sahoo A K 2020 Nanocomposite of Ag nanoparticles and catalytic fluorescent carbon dots for synergistic bactericidal activity through enhanced reactive oxygen species generation *Nanotechnology* **31**

[295] Saharkhiz M J, Motamedi M, Zomorodian K, Pakshir K, Miri R and Hemyari K 2012 Chemical Composition, Antifungal and Antibiofilm Activities of the Essential Oil of Mentha piperita L. *ISRN Pharm.* **2012** 1–6

[296] Valussi M, Antonelli M, Donelli D and Firenzuoli F 2021 Appropriate use of essential oils and their components in the management of upper respiratory tract symptoms in patients with COVID-19 *J. Herb. Med.* **28**

[297] Beyki M, Zhaveh S, Khalili S T, Rahmani-Cherati T, Abollahi A, Bayat M, Tabatabaei M and Mohsenifar A 2014 Encapsulation of Mentha piperita essential oils in chitosan-cinnamic acid nanogel with enhanced antimicrobial activity against Aspergillus flavus *Ind. Crops Prod.* **54** 310–9

[298] Singh A, Verma A, Singh R, Sahoo A K and Samanta S K 2021 Combination therapy of biogenic C-dots and lysozyme for enhanced antibacterial and antibiofilm activity *Nanotechnology* **32**

[299] Sreenivasamurthy S A, Akhter F F, Akhter A, Su Y and Zhu D 2022 Cellular

mechanisms of biodegradable zinc and magnesium materials on promoting angiogenesis *Biomater. Adv.* **139** 213023

[300] Ribatti D 2017 The chick embryo chorioallantoic membrane (CAM) assay *Reprod. Toxicol.* **70** 97–101

[301] Buhr C R, Wiesmann N, Tanner R C, Brieger J and Eckrich J 2020 The chorioallantoic membrane assay in nanotoxicological research—an alternative for in vivo experimentation *Nanomaterials* **10** 1–16

[302] Vu B T, Shahin S A, Croissant J, Fatieiev Y, Matsumoto K, Le-Hoang Doan T, Yik T, Simargi S, Conteras A, Ratliff L, Jimenez C M, Raehm L, Khashab N, Durand J O, Glackin C and Tamanoi F 2018 Chick chorioallantoic membrane assay as an in vivo model to study the effect of nanoparticle-based anticancer drugs in ovarian cancer *Sci. Rep.* **8** 1–10

[303] Dehari D, Chaudhuri A, Kumar D N, Patil R, Gangwar M, Rastogi S, Kumar D, Nath G and Agrawal A K 2023 A Bacteriophage Microgel Effectively Treats the Multidrug-Resistant Acinetobacter baumannii Bacterial Infections in Burn Wounds *Pharmaceuticals* **16** 942

[304] Chen M X, Alexander K S and Baki G 2016 Formulation and Evaluation of Antibacterial Creams and Gels Containing Metal Ions for Topical Application *J. Pharm.* **2016** 1–10

[305] Sivaraj D, Noishiki C, Kosaric N, Kiwanuka H, Kussie H C, Henn D, Fischer K S, Trotsyuk A A, Greco A H, Kuehlmann B A, Quintero F, Leeolou M C, Granoski M B, Hostler A C, Hahn W W, Januszyk M, Murad F, Chen K and Gurtner G C 2023 Nitric oxide-releasing gel accelerates healing in a diabetic murine splinted excisional wound model *Front. Med.* **10** 1–7

[306] Kaltalioglu K 2023 Sinapic acid-loaded gel accelerates diabetic wound healing process by promoting re-epithelialization and attenuating oxidative stress in rats *Biomed. Pharmacother.* **163** 114788

[307] Manju S, Malaikozhundan B, Vijayakumar S, Shanthi S, Jaishabanu A, Ekambaram P and Vaseeharan B 2016 Antibacterial, antibiofilm and cytotoxic effects of Nigella sativa essential oil coated gold nanoparticles *Microb. Pathog.* **91** 129–35

[308] Su D, Zhang X, Wu A, Yan H, Liu Z, Wang L, Tian C and Fu H 2019 CoO-Mo2N hollow heterostructure for high-efficiency electrocatalytic hydrogen evolution reaction *NPG Asia Mater*. **11**

[309] Kumari S D C, Tharani C B, Narayanan N and Kumar C S 2013 Formulation and characterization of Methotrexate loaded sodium alginate chitosan Nanoparticles *Indian J. Res. Pharm. Biotechnol.* **1** 915–21

Appendix A:

(a)

(b)

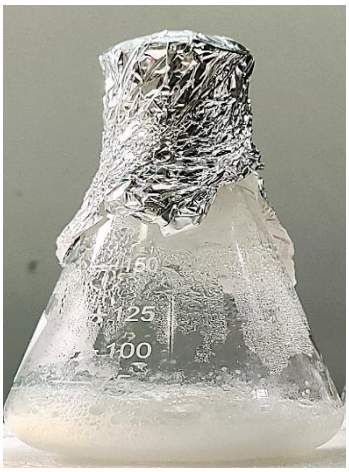

Coagulated Bovine Serum Albumin (BSA) with $MgCl_2$ Salt after 15 hr incubation at 55 °C

(c)

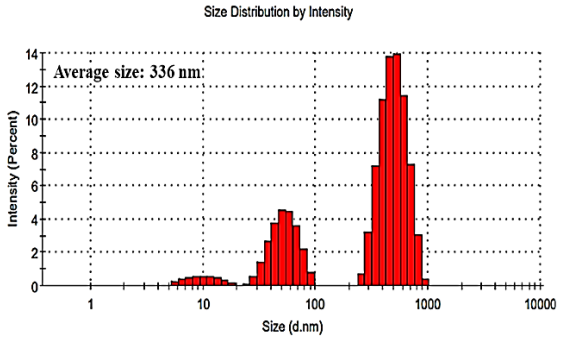

(d)

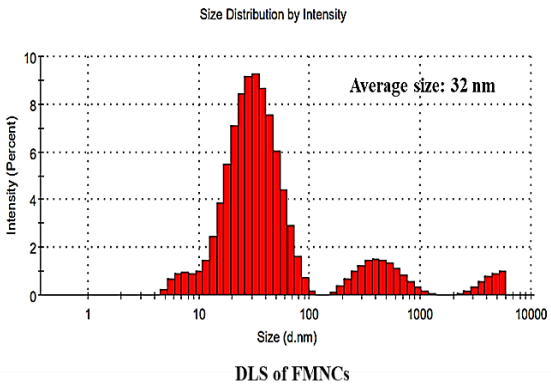

Figure. A1 (a) Image of FMNCs and Control 1 ($Mgcl_2$+ BSA) and control 2 ($Mgcl_2$ +Ascorbic acid), (b) Image of incubated $Mgcl_2$ + BSA at 55 °C, (C) DLS of control1 ($Mgcl_2$+ BSA), (d) DLS of FMNCs.

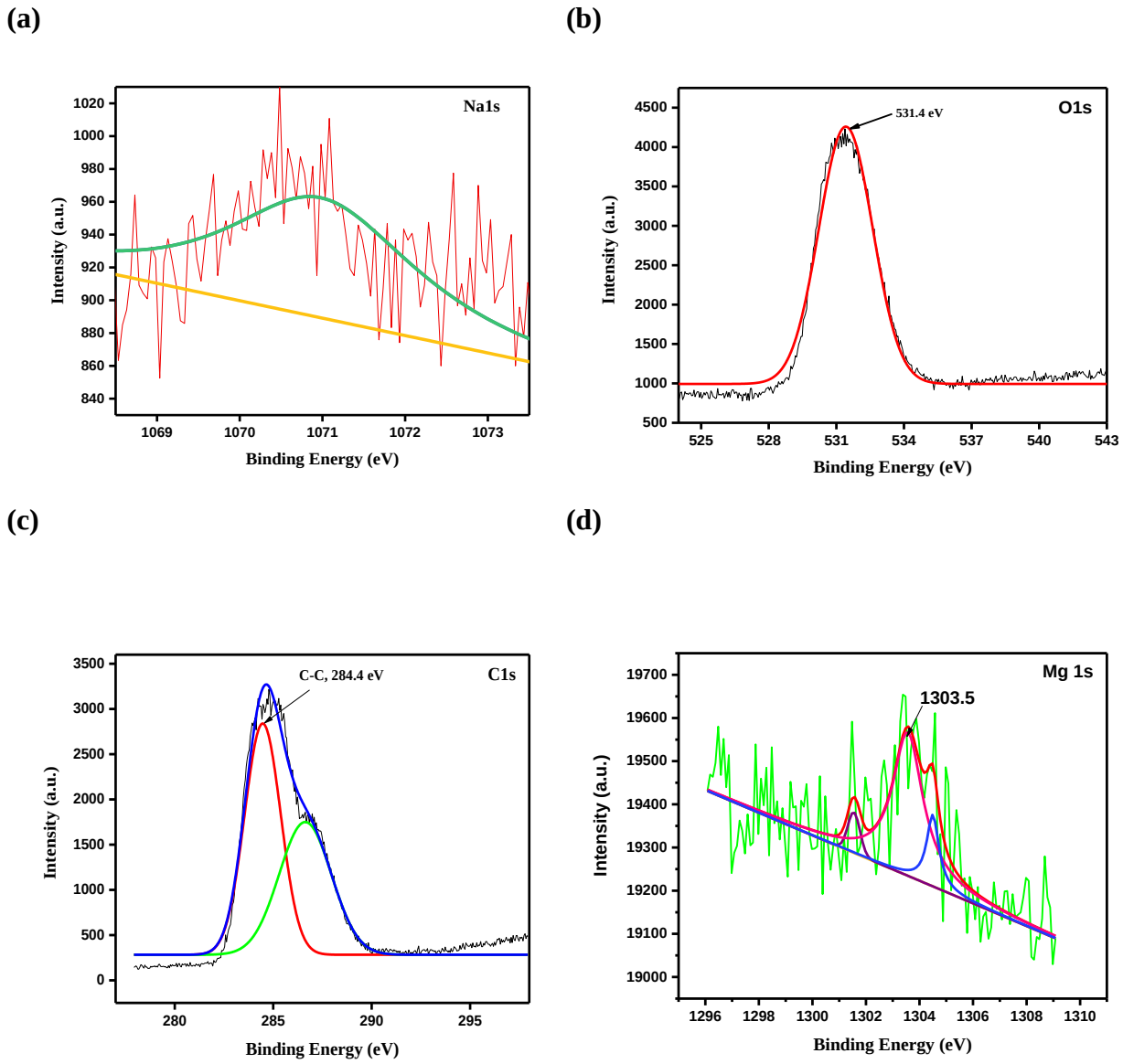

Figure. A2 XPS spectra of (a) Na 1s, (b) O 1s, (c) C 1s, (d) Mg 1s

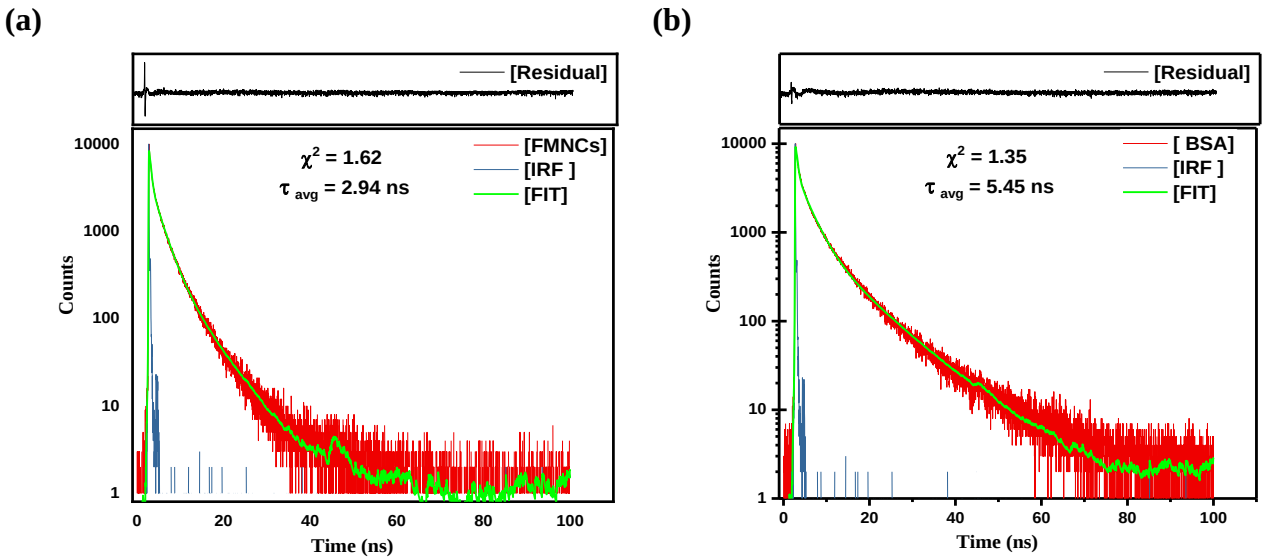

Figure. A3 (a) Fluorescence life time decay profile of FMNCs (λ_{Ex} 375 nm/λ_{Em} 459 nm). (b) Fluorescence life time decay profile of processed BSA protein under the same excitation value (λ_{Ex} 375 nm/λ_{Em} 459 nm)

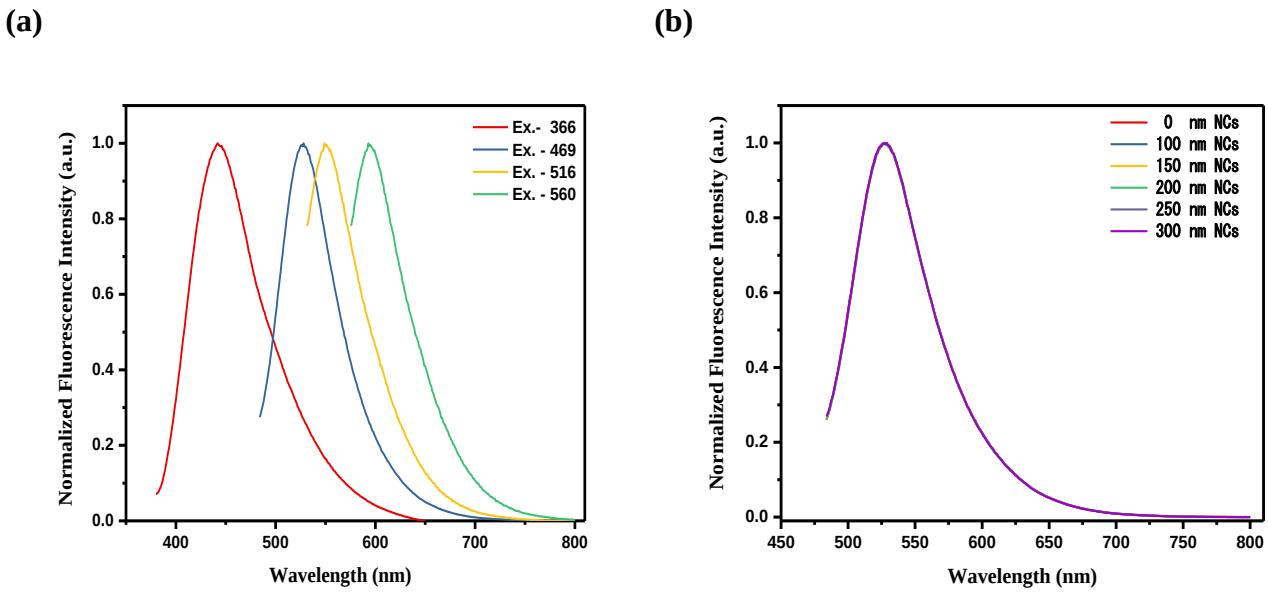

Figure. A4 (a) Normalized Fluorescence emission spectra of lyophilized FMNCs powder (one year old) at different excitations (366,469, 516 and 560). (b) Normalized fluorescence emission spectra of FMNCs after addition of various concentration of freshly prepared NaCl solution at λ_{Ex} 469.

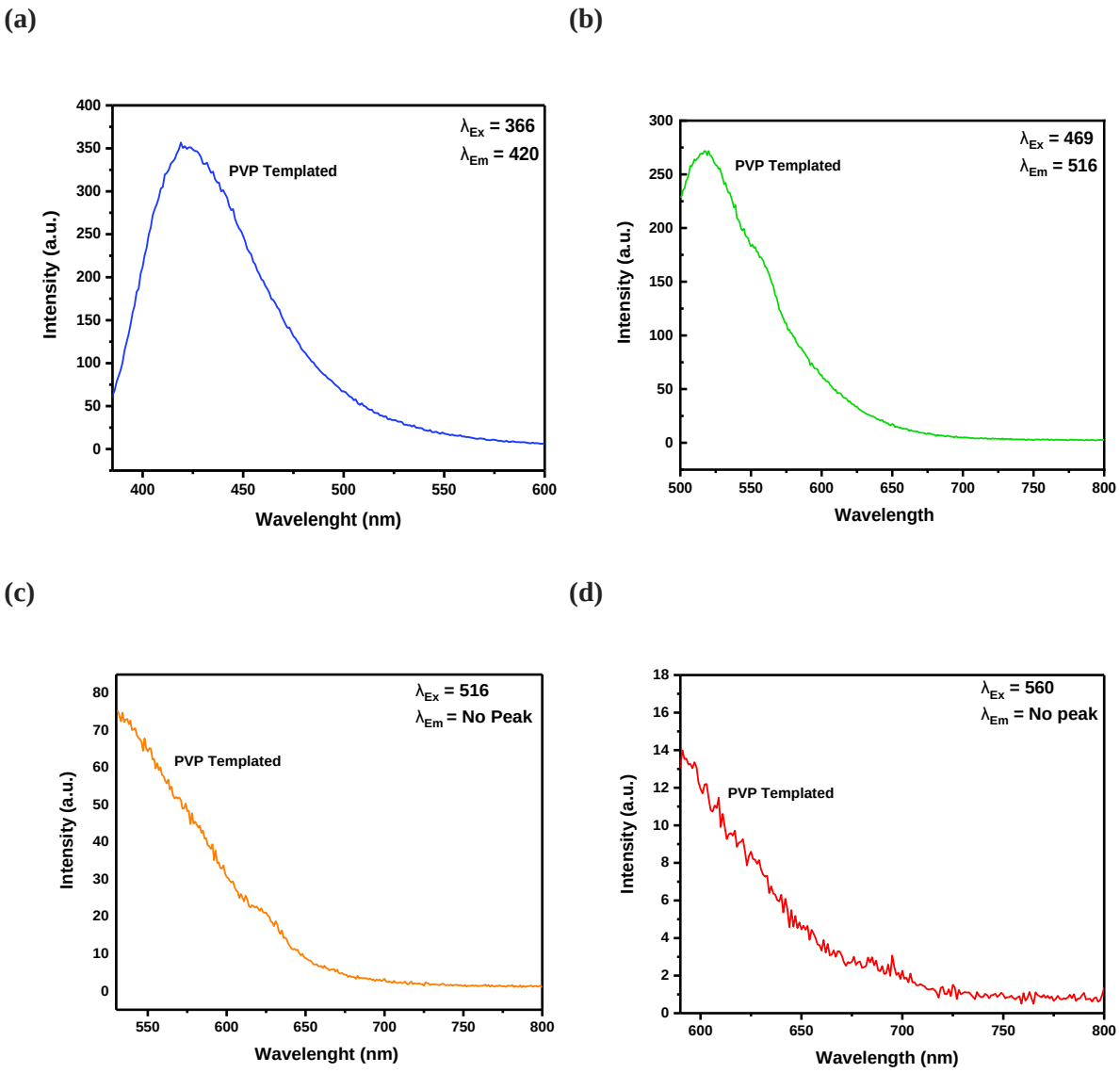

Figure. A5 (a) Fluorescence spectra of PVP templated FMNCs nanocluster at λ_{Ex} 366, (b) Fluorescence spectra of PVP templated FMNCs nanocluster at λ_{Ex} 469, (c) Fluorescence spectra of PVP templated FMNCs nanocluster at λ_{Ex} 516, (d) Fluorescence spectra of PVP templated FMNCs nanocluster at λ_{Ex} 560.

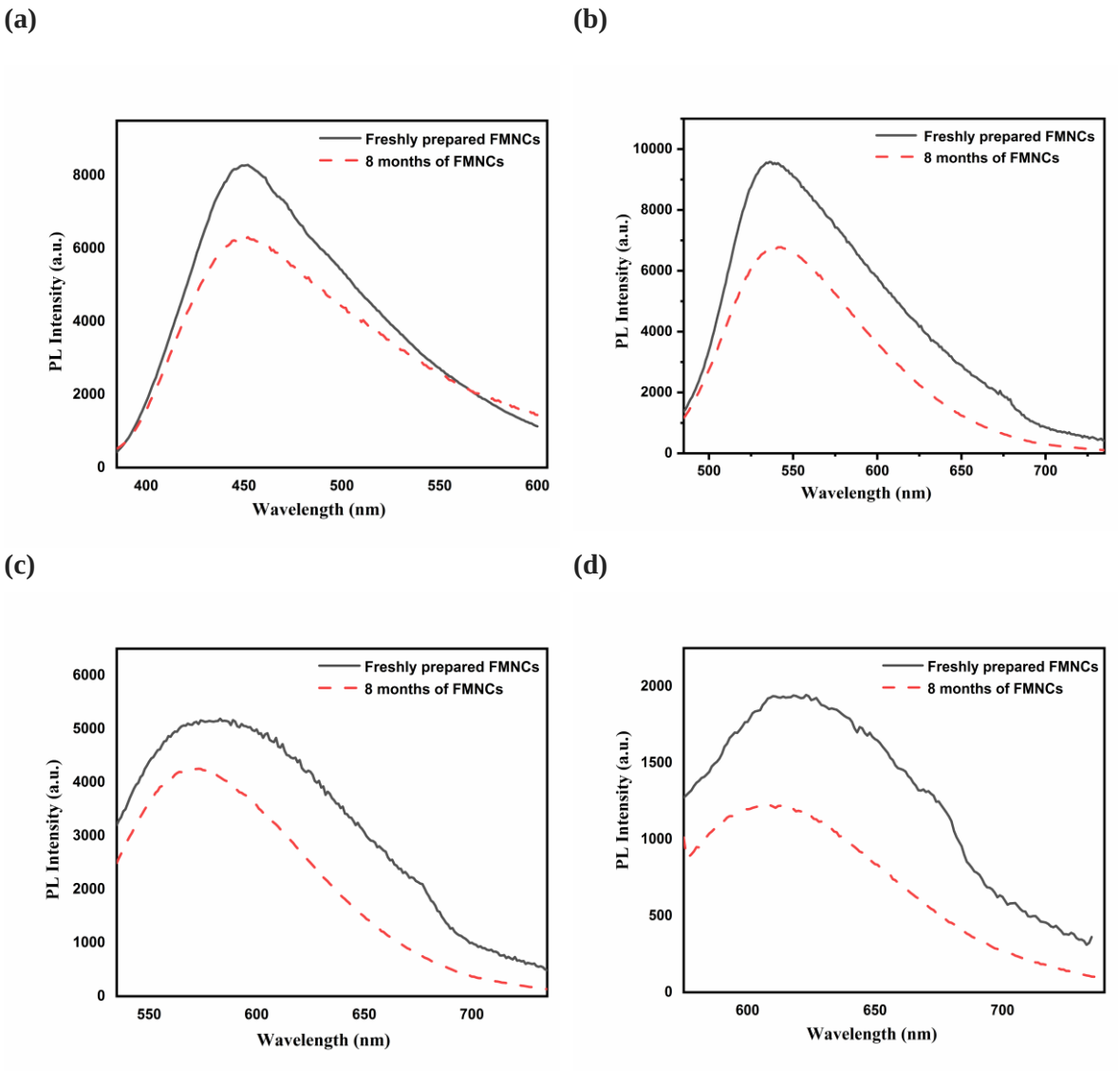

Figure. A6 (a) Fluorescence emission spectra of 8 months old and freshly prepared aqueous FMNCs at λ_{Ex} 366 (b) Fluorescence emission spectra of 8 months old and freshly prepared aqueous FMNCs at λ_{Ex} 469 (c) Fluorescence emission spectra of 8 months old and freshly prepared aqueous FMNCs at λ_{Ex} 516 (d) Fluorescence emission spectra of 8 months old and freshly prepared aqueous FMNCs at λ_{Ex} 560.

Appendix B

Figure B1

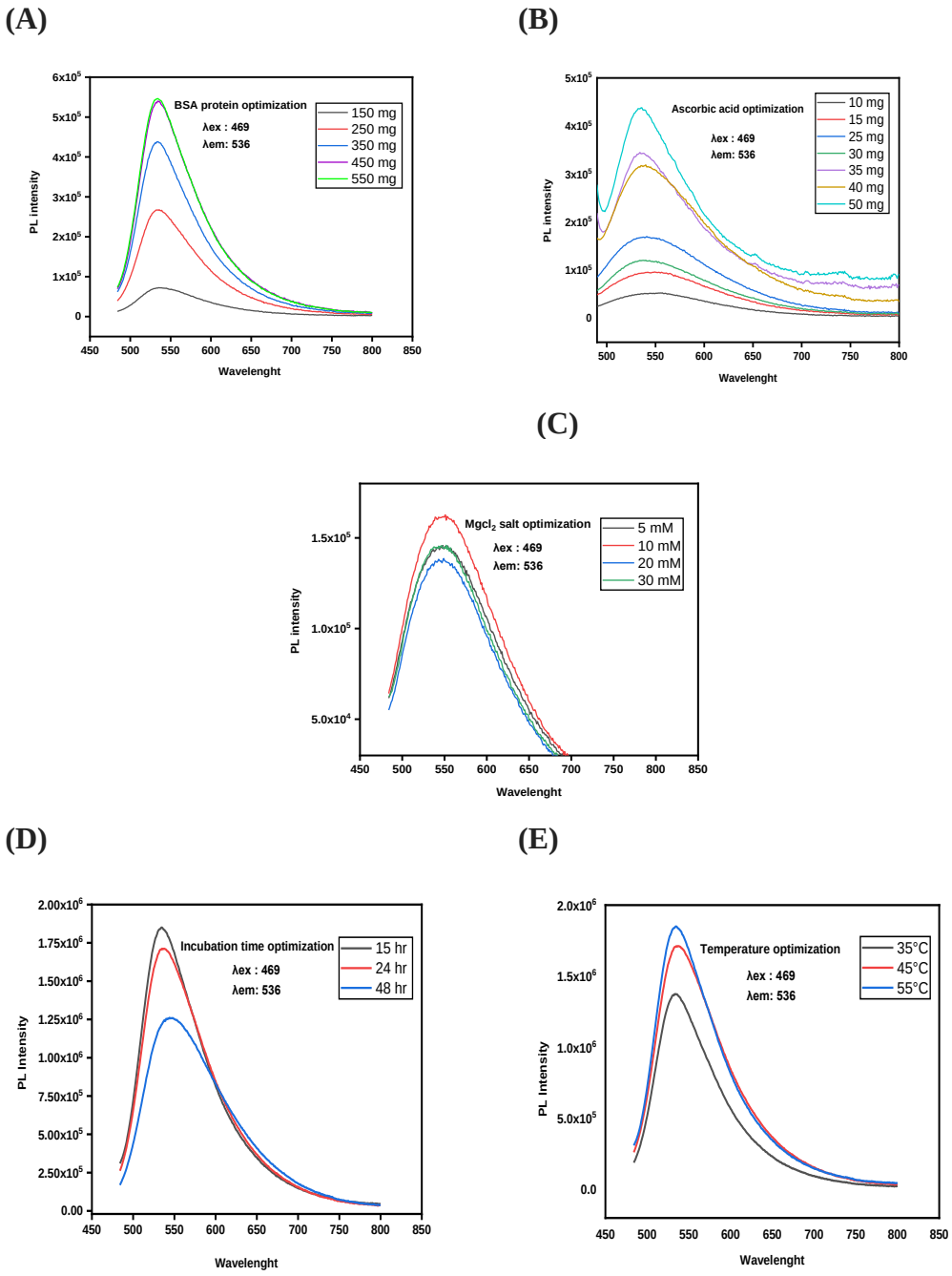

Figure B1 (A) BSA protein optimization (450 mg/ml optimized) (B) Ascorbic acid optimization (35 mg/ml optimized) (C) $Mgcl_2$ salt optimization (10mM optimized) (D) Incubation time optimization (15 hr. optimized) (E) Temperature optimization (55 ^{o} C optimized).

Nucleation models	**Model**	**Differential form f(α)**	**Integral form g(α)**
P2	Power Law	$(2/3)\ \alpha^{-1/2}$	$\alpha^{3/2}$
P3	Power Law	$2\alpha^{1/2}$	$\alpha^{1/2}$
P4	Power Law	$3\alpha^{2/3}$	$\alpha^{1/3}$
P5	Power Law	$4\alpha^{3/4}$	$\alpha^{1/4}$
Sigmoidal rate equations			
A1	Avarami-Erofeev	$(3/2)\ (1-\alpha)\ [-\ln(1-\alpha)]^{1/3}$	$[-\ln(1-\alpha)]^{2/3}$
A2	Avarami-Erofeev	$2(1-\alpha)\ [-\ln(1-\alpha)]^{1/2}$	$[-\ln(1-\alpha)]^{1/2}$
A3	Avarami-Erofeev	$3(1-\alpha)\ [-\ln(1-\alpha)]^{2/3}$	$[-\ln(1-\alpha)]^{1/3}$
A4	Avarami-Erofeev	$4(1-\alpha)\ [-\ln(1-\alpha)]^{3/4}$	$[-\ln(1-\alpha)]^{1/4}$
F1	Prout-Tompkins	$\alpha(1-\alpha)$	$\ln[\alpha/(1-\alpha)]$
F2	Contracting area	$2(1-\alpha)^{1/2}$	$1-(1-\alpha)^{1/2}$
F3	Contracting volume	$3(1-\alpha)^{2/3}$	$1-(1-\alpha)^{1/3}$
F4	Random nucleation (1)	$(1-\alpha)^2$	$1/(1-\alpha)$
F5	Random nucleation (2)	$(1-\alpha)^3/2$	$1/(1-\alpha)^2$
Diffusion models			
D1	1D diffusion	$1/2\alpha$	α^2
D2	2D diffusion-Valensi	$[-\ln(1-\alpha)]^{-1}$	$(1-\alpha)\ln(1-\alpha)+\alpha$
D3	3D diffusion-jander	$(3/2)\ (1-\alpha)^{2/3} / [1-(1-\alpha)^{1/3}]$	$[1-(1-\alpha)^{1/3}]^2$
D4	3D diffusion-Ginstling	$(3/2)/[(1-\alpha)^{-1/3} - 1]$	$1-2\ \alpha/3-(1-\alpha)^{2/3}$
Reaction order models			
R1	First order	$1-\alpha$	$-\ln(1-\alpha)$
R2	Second order	$(1-\alpha)^2$	$(1-\alpha)^{-1}-1$
R3	Third order	$(1-\alpha)^3$	$[(1-\alpha)^{-2}-1]/2$
R4	One and half order	$(1-\alpha)^{3/2}$	$2[(1-\alpha)^{-1/2}-1]$

Table B1

Table B2 Preexponential kinetic factor (A) at 10 ºC/min, computed by utilizing KAS-derived equation.

Conversion(α)	A (min^{-1})	A (Nuclei μm^{-2} min^{-1})
0.1	1.89077E+14	1.25645E+30
0.2	1.80698E+13	1.20077E+29
0.3	4.35197E+17	2.89E+33
0.4	3.61E+16	2.4E+32
0.5	7.8E+14	5.18E+30
0.6	1.29E+13	8.58E+28
0.7	9.63E+09	6.4E+25
0.8	4.92E+15	3.27E+31
0.9	778517597.8	5.1734E+24

Table B3 Nucleation rate computed by utilizing kinetic and thermodynamic barriers, essential for random nucleation process within MgNCs matrix.

T(K)	J ($nuclei$ $\mu m-2$ $min-1$) 10^0C/min	T(K)	J ($nuclei$ $\mu m-2$ $min-1$) 15^0C/min	T(K)	J ($nuclei$ $\mu m-2$ $min-1$) 20^0C/min
533.15	0.158867	539.22	0.4431	543.29	0.6007
570.19	16.63	576.16	42.191	579.24	45.84
587.18	128.59	594.24	351.78	597.24	376.76
600.17	451.47	608.17	1298.47	612.24	1570.89
616.23	1639.61	626.26	5360.72	630.29	6459.00
644.15	7461	658.24	29338.92	664.24	41301.41
697.21	5221919	705.16	11849271	712.16	16233076
777.18	19799076	795.16	65536129	807.21	1.11×10^8

Table B4 Value of exponential function constant Q_1, Q_2, ρ_1, and $\rho 2$, acquired from a theoretical model by fitting the experimental data.

Exponential function constants	10 ºC/min	15 ºC/min	20 ºC/min
Q_1	587.11	918.573	879.90
ρ_1	58.37	51.31	48.69
Y_o	-898778.80	-1648835.36	-1985815.90
Q_2	28.11	18.27	11.12
ρ_2	0.071±0.00642	0.05749±0.0029	0.05169±0.00191
J_o	-191008.20	-315372.41	-358593.10

** Q_1 and ρ_1 are exponential functions constant and Y_o is intercept for a theoretical model of nucleation vs temperature, whereas Q_2, ρ_2 and are exponential function constant and J_o is intercept for nucleation vs conversion.

Table B 5 Interfacial energy was calculated by using a thermodynamic barrier within the MgNCs matrix with respect to temperature.

T(K)	**ϒ (mJ/m2)-10^0C/min**	**T(K)**	**ϒ (mJ/m2)-15^0C/min**	**T(K)**	**ϒ (mJ/m2)-20^0C/min**
473.21	111.75	479.22	112.81	481.25	113.03
533.15	114.66	539.22	115.388	543.29	116.09
570.19	119.56	576.16	120.23	579.24	120.79
587.18	122.00	594.24	122.82	597.24	123.36
600.17	123.93	608.17	124.87	612.24	125.56
616.23	126.30	626.26	127.50	630.29	128.19
644.15	130.44	658.24	132.18	664.24	133.13
697.21	136.88	705.16	137.74	712.16	138.80
777.18	148.01	795.16	150.09	807.21	151.78

Section B1 Calculation of α – helix content using CD Spectra:

The α-helix content of BSA and FMNCs is calculated by using the following equation: -

$$\%\, helix = \left(\frac{\theta_{mrd} - 4000}{33000 - 4000}\right) \times 100$$

θ_{mrd} is the mean molar ellipticity per residue (deg cm^2/dmol)

$$\theta_{mrd} = \frac{\theta_d M}{10\, ncl}$$

θ_d is ellipticity in mdeg, M is the molecular weight of BSA in Da, c is concentration in mg/ml and l is path length in cm.

In this particular calculation:

M= 66050 Da, c= 0.5mg/ml (Pure BSA) and 0.4 mg/ml (MgNCs) and n is 583 (Amino acid residue in BSA)

The calculated α helicity was found to be 57.7% for Pure BSA, which becomes 22% after MgNCs formation, this result shows a drastic change in the conformation of BSA after MgNCs formation.

Section B2 Calculation ΔG* using CNT (Classical nucleation Theory) and Thermogravimetric analysis (TGA):

The Nucleation Rate for thermally activated process can be expressed as *(J. W. Mullin, Crystallization, Butterworth-Heinemann, Oxford, 1993)(Mullin):*

$$J = Aexp(\Delta G^*/kT) \qquad (1)$$

Where, k is Boltzmann constant ($1.3805 \times 10^{-23} JK^{-1}$), T is temperature, and $\Delta G^*$is critical free energy barrier to nucleation.

We assume that,

$$\text{Per molecule gas constant in 1 Mg cluster} = R/N_A = k \qquad (2)$$

Where, R is universal gas constant (8.314 J K^{-1} mol^{-1}), and N is Avogadro number (6.023×10^{23} mol^{-1}). *(J. W. Mullin, Crystallization, Butterworth-Heinemann, Oxford, 1993)(Mullin):*

Hence,

We can write $N_A = R$ (3)

$$6.023 \times 10^{23}\ mol^{-1} = R \qquad (4)$$

Now, 6.023×10^{23} mol^{-1} Mg clusters are nucleating at particular temperature (T) and respective conversion (α). So from eq. 2 we can write

$$6.023 \times 10^{23}\ \text{mol}^{-1} \rightarrow \frac{R}{N_A} \times N_A = k \qquad (5)$$

Hence,

$$1\ Mole\ of\ Mg\ Clusters \rightarrow k = R \qquad (6)$$

Putting the value of eq (6) in eq. (1) for nucleation of 1 mole of the particles eq. (7) is derived below.

$$J = Aexp(\Delta G^*/RT) \qquad (7)$$

But, in eq. (1) and eq. (7), while computation of nucleation rate, only A (Pre-exponential factor) is used during computation of kinetic barrier of nucleation, and activation energy of nucleation (E_α) is still missing. Thus, to compute nucleation rate, both kinetic and thermodynamic barriers were taken into account and expressed as below(Hu et al., 2012):

$$J = Aexp\left(\frac{-E}{kT}\right)exp\left(\frac{-\Delta G^*}{kT}\right) \quad (8)$$

To convert eq. (8) in terms of R, we will have to use k=R from eq. (6) thus by using eq. (6) in eq. (8), the nucleation rate equation gets converted in terms of R as follows:'

$$J = Aexp\left(\frac{-E}{RT}\right)exp\left(\frac{-\Delta G^*}{RT}\right) \quad (9)$$

Same eq. (9) is used to calculate nucleation rate by Qingyun Li et.al.

Thus, in current research, we are using eq. (9) for computation of nucleation rate. As our research goal is to calculate nucleation rate by TGA iso-conversional models at high temperature, the E is converted toE_α, A is converted to A_α and ΔG^* is also computed iso-conversionally, and finally eq. (9) can be expressed as by equation below:

$$J = A_\alpha exp\left(\frac{E_\alpha}{RT}\right)exp\left(\frac{\Delta G^*}{RT}\right) \quad (10)$$

The thermodynamic barrier ΔG^* can be expressed as below: (J. W. Mullin, Crystallization, Butterworth-Heinemann, Oxford, 1993)

$$\Delta G^* = \frac{16\pi\gamma^3 v^2}{3(kTlnS)^2} \quad (11)$$

After putting eq. (11) into eq. (8), we get, J as

$$J = Aexp\left(\frac{-E}{kT}\right)exp\left(\frac{-16\pi\gamma^3 v^2}{3k^3T^3(lnS)^2}\right) \quad (12)$$

In eq. (12), the thermodynamic barrier to nucleation rate is expressed as

$$B^* = \frac{16\pi v^2 \gamma^3}{3k^3T^3\,(lnS)^2} \qquad (13)$$

In our study, by examining z(α) master plots, it is already verified that our nucleation is random. In random nucleation process, during the formation of first nuclei, the nucleation is observed only, when the nuclei size (r) is equal to the standard critical size of nuleation (r*), according to the equation below(Dirksen and Ring, 1991):

$$r^* = \frac{2\beta_a \gamma v}{3\beta_v k_B T ln(S)} \qquad (14)$$

Where, β_a is 4π, β_v is 4π/3, γ is surface free energy per unit area, v is volume of aggregate, S is supersaturation, and T is temperature. When radius of nuclei formed becomes equal to the standard critical size of nucleation, as per eq. (13), the first nuclei formation takes place at particular temperature and the value of supersaturation (S) becomes 2.718 (Dirksen and Ring, 1991).

In our research, we are observing nuclei formation by R3 mechanism ($z(\alpha)$ master plots), as a starting phase of nucleation (when actual nucleation starts), thus in our case the value of supersaturation, S is 2.718.

By putting the value of S=2.718, the thermodynamic term B^* in eq. (13) becomes,

$$B^* = \frac{16\pi v^2 \gamma^3}{3k^3T^3\,(ln2.718)^2}$$

$$B^* = \frac{16\pi v^2 \gamma^3}{3k^3T^3\,(1)^2}$$

$$B^* = \frac{16\pi v^2 \gamma^3}{3k^3T^3} \qquad (15)$$

This eq. (15) is also used as a thermodynamic term, during estimation of nucleation kinetics of a L-glutamic acid (Lindenberg and Mazzotti, 2009). This thermodynamic term in eq. (15) is used to estimate interfacial energy variation with temperature.

The unit of R.H.S. of eq. (15) is

$$\frac{16\pi v^2\gamma^3}{3k^3T^3} = \frac{(m^3)^2 \times \left(\frac{J}{m^2}\right)^3}{\left(\frac{J}{K}\right)^3 \times K^3} = (unitless)$$

Thus, we adopted L.H.S of eq. (15) to be as.

$$\frac{\Delta G^*}{RT} = \frac{\left(\frac{J}{mol}\right)}{\left(\frac{J}{mol\,K}\right) \times K} = (unitless)$$

Thus, eq. (15) is expressed as,

$$\frac{\Delta G^*}{RT} = \frac{16\pi v^2\gamma^3}{3k^3T^3} \quad (16)$$

Thus, the eq. (16) is used to calculate interfacial energy against temperature.

The current nucleation of ultrasmall magnesium clusters is highly dependent on the temperature, and thereby TGA technology is used to understand the nucleation kinetics of ultrasmall magnesium clusters. During calculation of thermodynamic barrier(ΔG^*), eq. (11) is used. The calculated value of (ΔG^*) from eq. (11) is called as a free energy barrier to the nucleation at high temperature(Singh et al., 2021b). As this J in eq. (10) is used to compute nucleation rate against conversion (0.1 to 0.9), thus E_α and ΔG^* need to be calculated against conversion varying from 0.1 to 0.9 by TGA. Thus, by TGA for the calculation of free energy barrier to nucleation (ΔG^*) against conversion is used. To compute interfacial energy, eq. (16) is used:

$$\frac{\Delta G^*}{RT} = \frac{16\pi v^2\gamma^3}{3k^3T^3}$$

$$\frac{3k^3T^3\,\Delta G^*}{16RT\pi v^2} = \gamma^3$$

$$\gamma = \left(\frac{3k^3T^3\,\Delta G^*}{16RT\pi v^2}\right)^{1/3} \quad (17)$$

At 0.5 conversion and corresponding temperature of 600.17 K, eq. (17) can be computed as follows,

$$\gamma = \left(\frac{3 \times (1.38 \times 10^{-20})^3 \times (600.17)^3 \times 1.51 \times 10^8}{16 \times 8314 \times 600.17 \times 3.14 \times (2.32 \times 10^{-29})^2}\right)^{1/3}$$

$$= \left(\frac{2.5737 \times 10^{-43}}{1.3493 \times 10^{-49}}\right)^{1/3}$$

$$= (1907433.484)^{1/3}$$

$$= 124.017\, mJ/m^2$$

At 600.17 K, from eq. (10), according to Classical Nucleation Theory (CNT), we get

$$(B^*)_{CNT} = \frac{16\pi v^2 \gamma^3}{3k^3T^3\,(lnS)^2}$$

$$\frac{\Delta G^*_{CNT}}{RT} = \frac{16\pi v^2 \gamma^3}{3k^3T^3\,(lnS)^2}$$

$$\Delta G^*_{CNT} = \frac{16\pi v^2 \gamma^3 RT}{3k^3T^3\,(lnS)^2}$$

At 600.17 K, ΔG^*_{CNT} is expressed as,

$$\Delta G^*_{CNT} = \frac{16\pi v^2 \gamma^3 RT}{3k^3T^3\,(lnS)^2}$$

$$= \frac{16 \times 3.14 \times (2.32 \times 10^{-29})^2 \times (124.017)^3 \times 8314 \times 600.17}{3 \times (1.38 \times 10^{-20})^3 \times (600.17)^3 \times (ln2.718)^2}$$

$$= \frac{2.573674 \times 10^{-43}}{1.704438 \times 10^{-51}}$$

$$= 150998393.61 mJ/mol$$

$$\Delta G^*_{CNT} = 150.998 kJ/mol$$

At 600.17 K, Free energy change of nucleation by TGA (ΔG^*_{TGA}) is expressed as,

$$\Delta G^*_{TGA} = E_\alpha + RT_p ln\left(\frac{K_B T_p}{hA}\right)$$

$$= E_\alpha + RT_p ln\left(\frac{K_B T_p}{hA}\right)$$

Where E_α = Activation energy at particular conversion in Joules/mole, k is Boltzmann constant ($1.3805 \times 10^{-23} JK^{-1}$), R molar gas constant (8.314 Joules/K-mole)

$$= 171401 + 8.314 \times 592.05 ln\left(\frac{1.380649 \times 10^{-23} \times 592.05}{(6.626 \times 10^{-34}) \times (7.8 \times 10^{14})}\right)$$

$$= 171401 + 8.314 \times 592.05 \ln\left(\frac{8.17413 \times 10^{-21}}{5.16828 \times 10^{-19}}\right)$$

$$= 171401 + 8.314 \times 592.05 \times \ln 0.0158159$$

$$= 171401 + 8.314 \times 592.05 \times (-4.1467)$$

$$= 171401 - 20411.316$$

$$= 150989 J/mol$$

$$\Delta G^*_{TGA} = 150.989 kJ/mol$$

Hence it is proved at 0.5 conversion and 600.17K, ΔG^* calculated from Classical Nucleation Theory ($\Delta G^*_{CNT} = 150.998 kJ/mol$) and TGA technique ($\Delta G^*_{TGA} = 150.989 kJ/mol$) comes out to be same.

Appendix C

(a) **(b)**

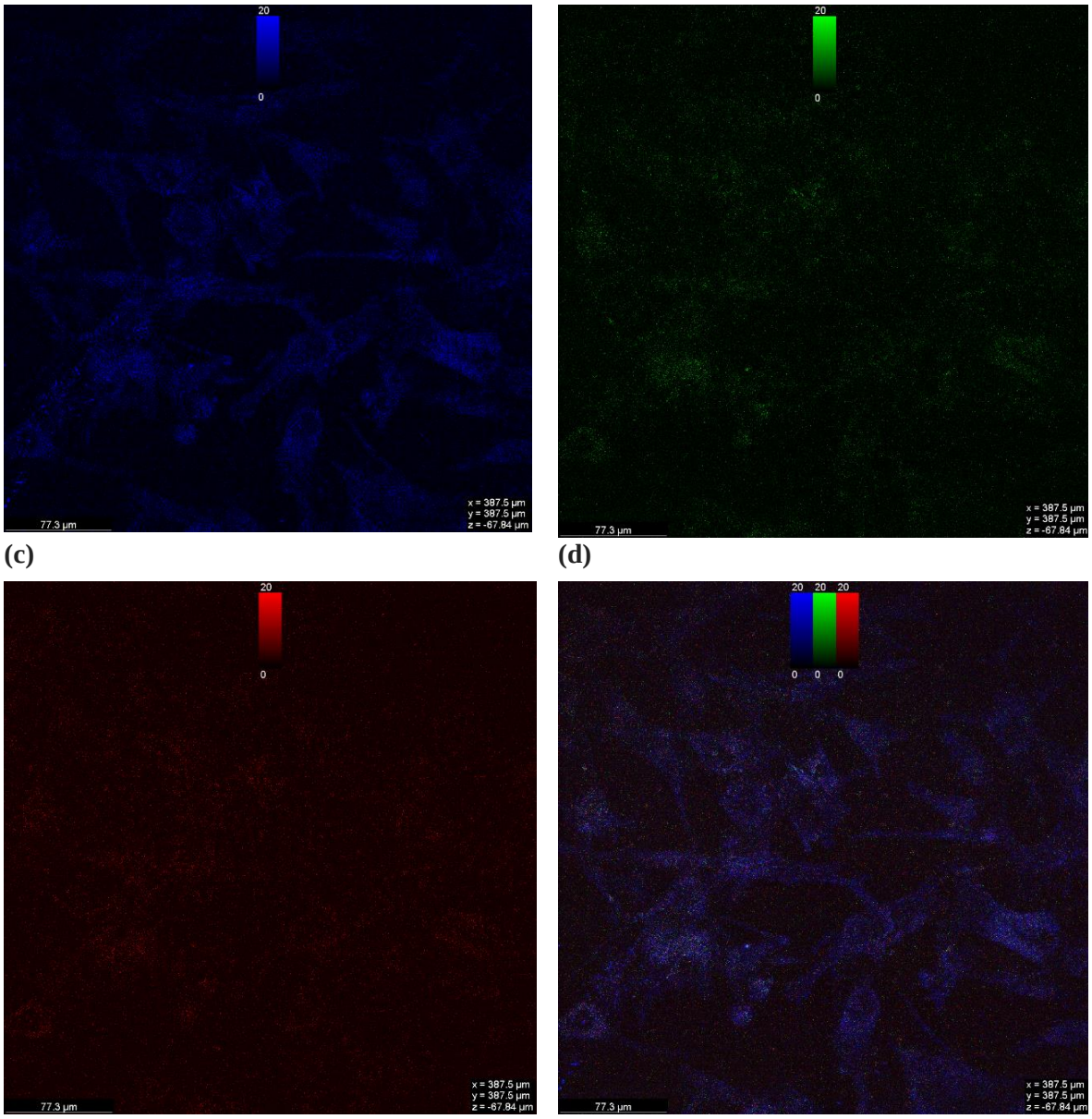

(c) **(d)**

Figure. C1 Multifluorescent confocal image of U 87-MG cells treated with Lysozyme.

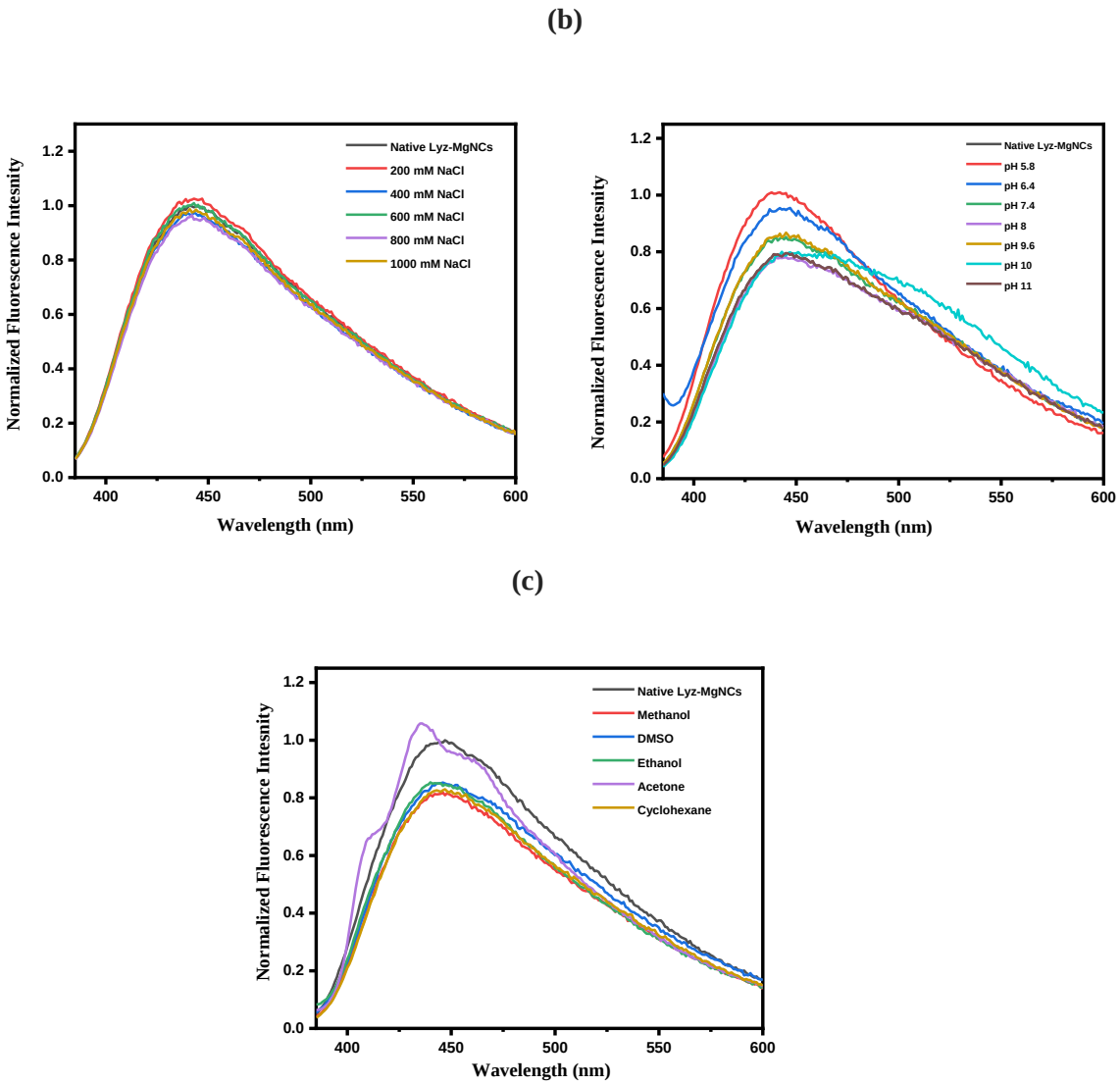

Figure. C2 (a) Normalized fluorescence emission spectra of Lyz-MgNCs after addition of various concentration of freshly prepared NaCl solution at λ_{Ex} 366 nm, (b) pH. Dependent Fluorescence emission spectra at different pH. (5.8-11) Values at λ_{Ex} 366 nm, (c) Normalized fluorescence intensity of Lyz-MgNCs with different solvents at λ_{Ex} 366 nm

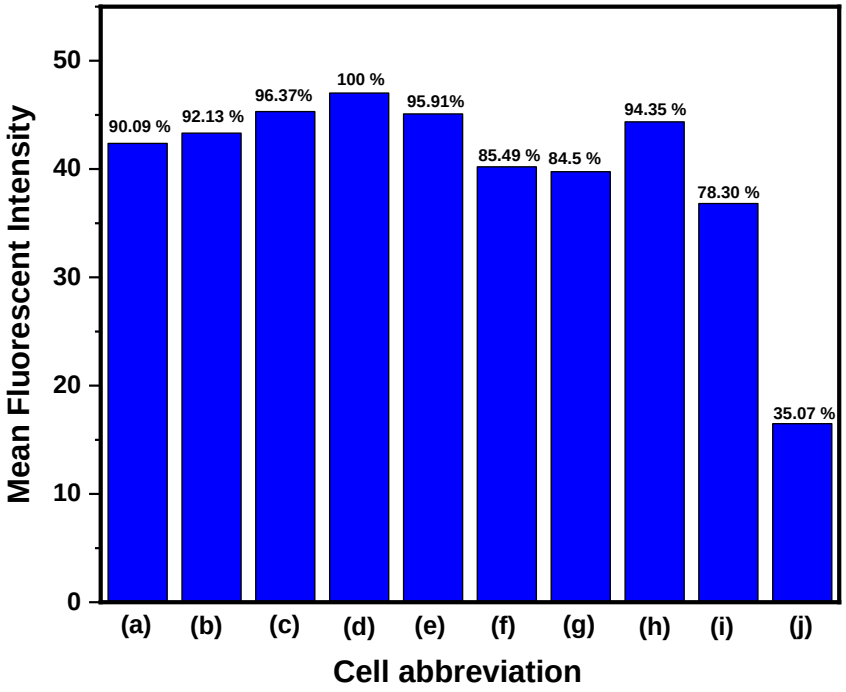

Figure. C3 Mean Luminescence Intensity in U -87 MG cells (1) Lyz-MgNCs [Ex. 366 nm, Em. Blue (450 nm)] ((a) = 0 µm, (b) = 2µm, (c) = 4µm, (d) = 6µm, (e) = 8µm, (f) = 10µm, (g) = 12µm, (h) = 14 µm, (i) = 16 µm, (j) = 18 µm.

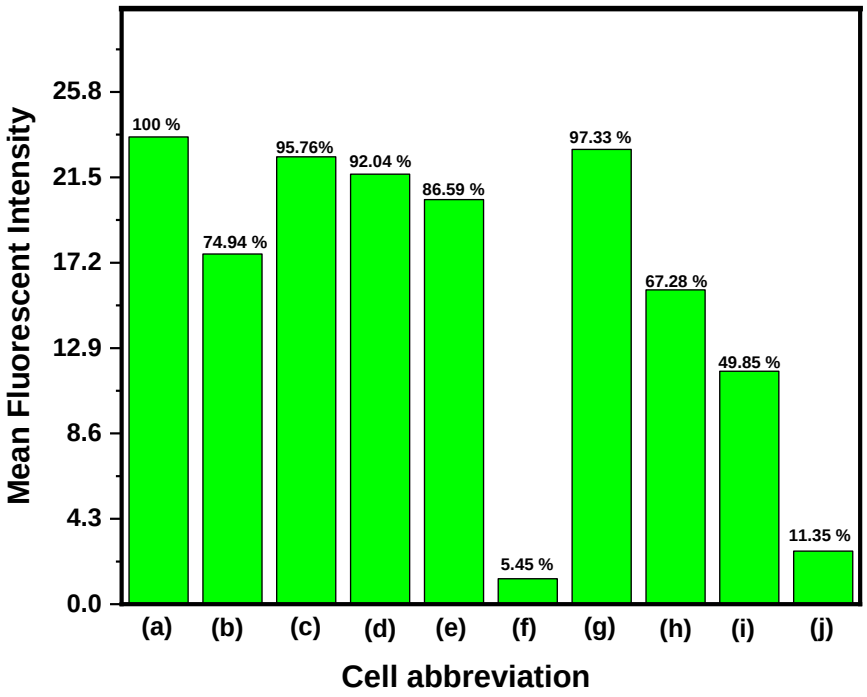

Figure. C4 Mean Luminescence Intensity in U -87 MG cells Lyz-MgNCs [Ex. 469 nm, Em. Green (545 nm)] ((a) = 0 µm, (b) = 2µm, (c) = 4µm, (d) = 6µm, (e) = 8µm, (f) = 10µm, (g) = 12µm, (h) = 14 µm, (i) = 16 µm, (j) = 18 µm

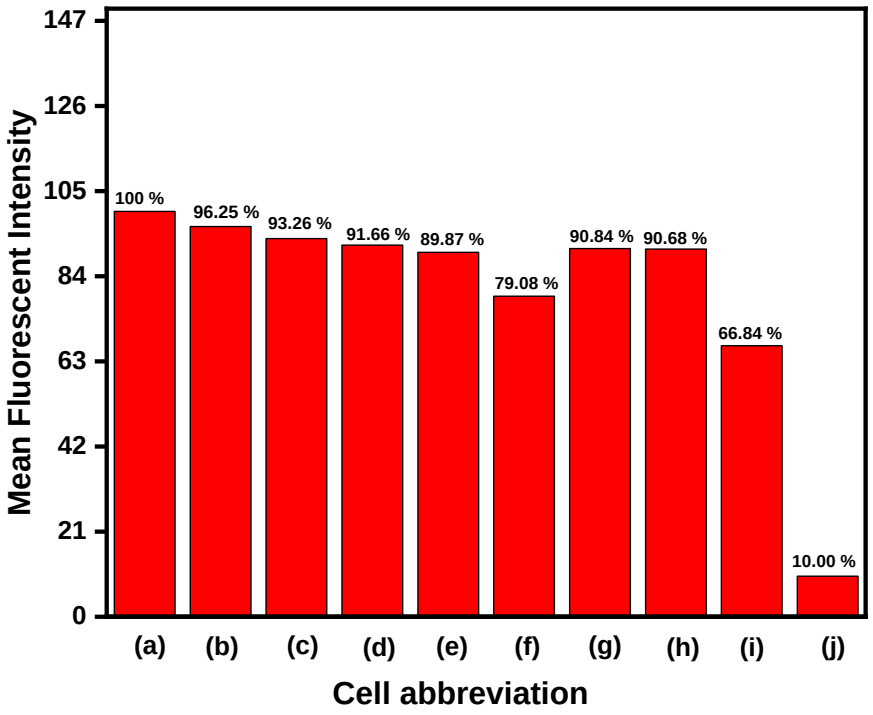

Figure. C5 Mean Luminescence Intensity in U -87 MG cells Lyz-MgNCs [Ex. 560 nm, Em. Red (628 nm)] ((a) = 0 µm, (b) = 2µm, (c) = 4µm, (d) = 6µm, (e) = 8µm, (f) = 10µm, (g) = 12µm, (h) = 14 µm, (i) = 16 µm, (j) = 18 µm

1. **Prachi Srivastava**, Vivek Kumar Verma, Shivesh Sabbarwal, Mamata Singh, Kedar Sahoo, Dr. Biplob Koch, Dr. Manoj Kumar. "White Light Emitting, Biocompatible, Water Soluble Metallic Magnesium Nanoclusters for Bioimaging Applications." Nanotechnology I.F 3.99.
2. **Prachi Srivastava**, Shivesh Sabbarwal, Vivek Kumar Verma, Dr. Manoj Kumar "A novel approach for determination of Nucleation Rates and Interfacial Energy of Metallic Magnesium Nanoclusters at High Temperature using Non-isothermal TGA Models." Chemical Engineering Science (2022): 118223. I.F 4.89
3. Vivek Kumar Verma, **Prachi Srivastava**, Shivesh Sabbarwal, Mamata Singh, Dr. Biplob Koch, Dr. Manoj Kumar "White Light Emitting Gd_2O_3 Nanoclusters for In-vitro Bioimaging". ChemistrySelect I.F 2.3.
4. Shivesh Sabbarwal, **Prachi Srivastava**, Vivek Kumar Verma, Dr. Manoj Kumar "New Approach to Calculate the Kinetic and Thermodynamic Barriers for Computation of Nucleation Rates and Interfacial Energy of $CaCO_3$ Prenucleation Nanoclusters at High Temperature using TGA models and their In-Situ Crystallization" Crystal Research and Engineering I.F 1.6
5. Vivek Kumar Verma, Shivesh Sabbarwal, **Prachi Srivastava**, Dr. Manoj Kumar "In-Depth Insight of Thermodynamic and Kinetic Barrier for Computation of Nucleation Rate and Interfacial Energy of Ultra-Small Gd_2O_3 Nanoclusters Utilizing Non-Isothermal Thermogravimetric Models". Physica Scripta I.F 3.1.
6. **Srivastava, Prachi**, et al." Design and development of photothermally active Ag3Mg bimetallic nanoparticles as antimicrobial synergistic combination therapies against clinically relevant pathogens" Nanoscale. IF 10.5 (Submitted)

7. **Srivastava, Prachi**, et al.” Essential oil mediated synthesis of angiogenetic Magnogel against clinically relevant pathogens microbes and for wound healing” Colloids and Surfaces B: Biointerfaces. IF 5.8 (Submitted)
8. **Srivastava, Prachi**, et al.” Bright fluorescent lysozyme templated magnesium nanoclusters for brain-cell and In-vivo live imaging applications.” Colloids and Surfaces B: Biointerfaces. IF 5.9 (Submitted).
9. Vivek Kumar Verma**, Prachi Srivastava**, Shivesh Sabbarwal, Mamata Singh, Dr. Biplob Koch, Dr. Manoj Kumar “One-pot synthesis of ultra-fine but ultra-effective Chitosan targeted gadolinium oxide nanocluster for multimodal imaging" Colloids and Surfaces B: Biointerfaces. I.F 6.4 (submitted).
10. Shivesh Sabbarwal, Vivek Kumar Verma, Shreyashi Majumdar, **Prachi Srivastava**, Manoj Kumar “A Facile Synthesis of Nanodiamond Sn nanocrystals at room temperature with their beta phase for in-vitro photothermal cancer research. in-vivo toxicology and integrated Fourier transform modeling” ACS Material Letter I.F 8.4 (Under review)